N O T I C E

THIS DOCUMENT HAS BEEN REPRODUCED FROM
MICROFICHE. ALTHOUGH IT IS RECOGNIZED THAT
CERTAIN PORTIONS ARE ILLEGIBLE, IT IS BEING RELEASED
IN THE INTEREST OF MAKING AVAILABLE AS MUCH
INFORMATION AS POSSIBLE

NASA

Technical Memorandum 82146

Magnetic Field of Jupiter:
A Generalized Inverse Approach

J.E.P. Connerney

JUNE 1981

THE MAGNETIC FIELD OF JUPITER: A GENERALIZED INVERSE APPROACH

J. E. P. Connerney*
Planetary Magnetospheres Branch
Laboratory for Extraterrestrial Physics
NASA/Goddard Space Flight Center
Greenbelt, Maryland 20771

* NAS/NRC Resident Research Associate

ABSTRACT

The estimation of planetary magnetic fields from observations of the magnetic field gathered along a spacecraft flyby trajectory is examined with the aid of generalized inverse techniques, with application to the internal magnetic field of Jupiter. Model non-uniqueness resulting from the limited spatial extent of the observations and noise on the data is explored and quantitative estimates of the model parameter resolution are found. The presence of a substantial magnetic field of external origin due to the currents flowing in the Jovian magnetodisc is found to be an important source of error in estimates of the internal Jovian field, and new models explicitly incorporating these currents are proposed. New internal field models are derived using the vector helium magnetometer observations and the high field fluxgate observations of Pioneer 11, and knowledge of the external current system gained from the Pioneer 10 and Voyagers 1 and 2 encounters.

INTRODUCTION

Four spacecraft have thus far encountered Jupiter and permitted in situ investigation of many aspects of the Jovian system, including detailed observations of the inner magnetosphere. These spacecraft have explored different regions of the inner magnetosphere by virtue of their unique trajectories. The near-equatorial approach of Pioneer 10 to within 2.8 Jovian radii permitted the first observations of what has become known as the magnetodisc (Smith et al., 1974; Van Allen et al., 1974), a thin annular disc of tenuous plasma and charged particles encircling the giant planet to distances approaching 100 Jovian radii. Large scale azimuthal currents flowing in this magnetodisc, subsequently observed by the Voyagers 1 and 2 spacecraft (Ness et al., 1979a; Ness et al., 1979b; Bridge et al., 1979) lead to a substantial magnetic field of external origin throughout the entire inner magnetosphere. The high-inclination retrograde approach of the Pioneer 11 spacecraft yielded measurements of the inner magnetosphere at high latitudes spanning a wide range of Jovian longitude. In addition, the close approach of ∿1.6 Jovian radii (R_J) made this trajectory the most favorable for the purposes of estimating the internal magnetic field of Jupiter. Thus, models of the internal field based on the Pioneer 10 measurements (Smith et al., 1974) were quickly supplanted by models based on the Pioneer 11 observations

2

(Davis and Smith, 1976; Acuna and Ness, 1976). The near equatorial approaches of the Voyager 1 and 2 spacecraft, at the close approaches of ∿5 and 10 R_J, have permitted more detailed studies of the external azimuthal current system (Connerney et al., 1981) but have thus far added little to the present understanding of the internal magnetic field of Jupiter (Ness et al., 1979b).

As the number of available Jovian internal field models grows it becomes increasingly important to evaluate the model non-uniqueness inherent in the estimation of planetary magnetic fields from flyby observations. While some of the proposed models represented an intermediate stage of data processing and analysis, in general differences between the proposed models reflect differences in the number and kind of coefficients used in the basic models, differences in the actual observations, data intervals chosen for analysis, and the choice of weights applied to the observations in the least squares minimization process. A recent summary of the magnetic field observations of Jupiter (Smith and Gulkis, 1979) lists six spherical harmonic models of the Jovian magnetic field; five based on the Pioneer 10 and 11 vector helium magnetometer (VHM) data (Smith et al., 1974; Smith et al., 1976) and one derived from the Pioneer 11 fluxgate magnetometer (FGM) observations (Acuna and Ness, 1976). These models (with the exception of P10-11 combined models, e.g., Smith and Gulkis, 1979) all represent a 'good' fit along one trajectory in the sense of minimizing the weighted or unweighted model residuals, but lead to substantially different model fields in other regions of space.

The model non-uniqueness we refer to arises from the spatial limitations of the available observations and the noise on the data. In the usual spherical harmonic representation of planetary fields, there exist certain linear combinations of the model parameters which lead to a very small magnetic field along the spacecraft trajectory, but a large magnetic field elsewhere (e.g., at the planet's surface). That is, observations along a single flyby trajectory are insensitive to certain combinations of parameters. This basic lack of information, inherent in the available observations, leads to an unavoidable model non-uniqueness.

This paper concerns the estimation of planetary magnetic fields from flyby observations, in particular from the Pioneer 11 flyby of Jupiter in

3

December 1974. The non-uniqueness of derived models will be examined utilizing the generalized inverse techniques that have been developed during the last decade in other branches of geophysics, notably, seismic data inversion (Wiggins, 1972), gravity and magnetics (Pedersen, 1977), and studies of the electrical conductivity of the earth (Johansen, 1977). The generalized inverse techniques are of wide applicability in studying the often peculiar properties of linear (or linearized) systems and provide a framework for the evaluation of various models. The method underscores the uniqueness problems associated with the derivation of spherical harmonic expansions for the internal field and facilitates a systematic study of model parameter resolution. As the inevitable comparisons between models derived from different spacecraft flybys are made (e.g., Hide and Malin, 1979), it is important to evaluate the observations for consistency and develop models which are applicable to all of the flybys. The ultimate goal is to find one model, or field description, which is appropriate to all the observations, allowing integration of and sensible comparisons among the individual flybys. Thus, we will in addition examine the basic models chosen to represent the data and the validity of assumptions required by the conventional spherical harmonic analysis of these data. In this regard we will assess the importance of the magnetic field contribution due to external currents in the Jovian magnetodisc and propose improved models which explicitly incorporate these effects. For this purpose, models of the inner magnetosphere resulting from an analysis of Voyager 1, Voyager 2, and Pioneer 10 observations (Connerney et al., 1981) will be used to supplement the conventional spherical harmonic analysis.

The primary purpose of an internal field model is to provide an accurate description of the magnetic field throughout all space, not just along a single trajectory. Thus the ultimate test of a derived field model is how well it predicts the field in regions of space far removed from the locus of observations to which the model was fitted. Correlative data can be used to test various models, as well as additional in situ magnetic field observations. Comparison of predicted charge particle satellite absorption with observations (Acuna and Ness, 1976) is a powerful test of field models, since the trapped charged particle population reflects a global magnetic field topology rather than a localized observation. Indeed, satellite charged

particle absorption signatures can be used (Acuna et al., 1980) to constrain the initial field models. Other field topology diagnostics which have been applied to the Jovian field with varying success include ultraviolet auroral observations (Broadfoot et al., 1980), the polarization of Jovian decimetric radiation (Birmingham, 1980; de Pater, 1981) and the frequency and beaming pattern of decameter radio emission (Alexander et al., 1975). These observations can also in principle be used to constrain possible field models.

METHOD OF ANALYSIS

Increasingly more sophisticated models of the internal Jovian magnetic field have been proposed as the quantity and quality of available data increased. The Pioneer 10 data were initially modeled as a centered, tilted dipole and an offset, tilted dipole (Smith et al., 1974; Van Allen et al., 1974). Ultimately, data were interpreted utilizing the spherical harmonic analysis (Chapman and Bartels, 1940) conventionally used in studies of the earth's magnetic field. In the usual spherical harmonic analysis it is assumed that the data were obtained in a source free region of space (such that $\mu_o \underline{J} = \underline{\nabla} \times \underline{B} = 0$). The magnetic field $\underline{B}$ can then be expressed as the gradient of a scalar potential function

$$\underline{B} = -\nabla V = -\nabla(V^e + V^i) \tag{1}$$

which can be written as a sum of two potentials, representing sources internal and external to the region of interest. The potential is expanded in terms of spherical harmonics

$$V = V^e + V^i = a \sum_{n=1}^{\infty} (r/a)^n T_n^e + (a/r)^{n+1} T_n^i \tag{2}$$

where r is the distance to the planet's center, a is the planetary radius, and the T_n^e and T_n^i are given by

$$T_n^i = \sum_{m=0}^{n} p_n^m(\cos\theta) [g_n^m \cos m\phi + h_n^m \sin m\phi] \tag{3}$$

$$T_n^e = \sum_{m=0}^{n} P_n^m(\cos\theta) [G_n^m \cos m\phi + H_n^m \sin m\phi] \qquad (4)$$

where θ and ϕ are co-latitude and east longitude, respectively, the P_n^m are the associated Legendre functions with Schmidt normalization, and the g_n^m, h_n^m, G_n^m, H_n^m are the internal and external Schmidt coefficients. The series (2) is terminated at a suitable $n = n_{max}$ and the coefficients g_n^m, h_n^m, G_n^m, H_n^m are chosen to minimize, in a least squares sense, the differences between the model field and the observations. This is accomplished by solution of an overdetermined linear system

$$\bar{Y} = \bar{A}\,\bar{X} \qquad (5)$$

where $\bar{Y}$ is a column matrix of the N magnetic field observations, $\bar{A}$ is an N x M matrix relating the observations to the model parameters, $\bar{X}$, arranged as a length M column matrix of the g_n^m, h_n^m, G_n^m, H_n^m coefficients. The details of the usual least squares procedure in this application are summarized in Acuna and Ness (1976b).

The shortcomings of this usual spherical harmonic analysis as applied to the magnetic field observations at Jupiter have been discussed by both teams of investigators involved (Davis and Smith, 1976; Acuna and Ness, 1976b). Briefly, these shortcomings fall into two distinct areas which will be discussed separately. The first involves inadequacies of the basic model and the second involves the often peculiar properties of linear systems.

EXTERNAL FIELDS

Inadequacies in the basic model include the assumption that the data were obtained in a source-free space and the inefficiency of modeling fields due to external currents as an expansion of the form (2) with a limited number of terms. In the spherical harmonic analysis of Voyager 1 and 2 magnetic field data (Ness et al., 1979a,b) the reduced g_1^0 terms were attributed to the repeated passage of these spacecraft through an annular current sheet (i.e., the magnetodisc) circling Jupiter. It is now clear (Connerney et al., 1981) that Pioneer 10 and Voyagers 1 and 2 were repeatedly immersed in a current-

carrying region even as they traversed the innermost Jovian magnetosphere. Azimuthal current densities in the magnetic equatorial plane of $\sim 5 \times 10^6$ A/R_J^2 at a radial distance of 5 R_J were typical of models considered for both Voyager and Pioneer 10 encounters. Consequently, it is necessary to analyze these data in the context of a model which is applicable in a region of space containing sources. While it is quite possible that Pioneer 11 remained in source-free space during encounter, it is most probable that the magnetic field observations include a sizeable contribution from the external current system. Some of the 'systematic effects' in the residual (observed minus calculated field) noted by Davis and Smith (1976) in their analysis of the Pioneer 11 vector helium magnetometer data attest to the presence of this sheet perturbation field. For this encounter the problem is one of 'leakage' or aliasing of the field due to external currents into coefficients describing the internal field (g_n^m, h_n^m).

A reasonable starting point in the effort to construct improved models is to concatenate a spherical harmonic expansion of the type (2) containing only internal terms with an explicit model of the current system in the Jovian magnetosphere. While several models of the Jovian magnetosphere and external current system exist (Barish and Smith, 1975; Goertz et al., 1976; Jones et al. (1980); Beard and Jackson, 1976; Engle and Beard, 1980; Connerney et al., 1981) only the model of Connerney et al. (1981) represents a detailed vector fit to magnetometer observations in the innermost magnetosphere (< 20 R_J), the region of importance here. The other models represent qualitative fits (Beard and Jackson, 1976; Engle and Beard, 1980; Barish and Smith, 1976) or are applicable in the more distant magnetosphere (Goertz et al., 1976) and often match only scalar magnitude. The Euler potential models of Goertz et al. (1976) and Jones et al. (1980) are valid only in the near equatorial region of the distant (R > 20) magnetosphere, while the Biot-Savart model of Jones et al. (1980) was compared only with observations obtained at radial distances exceeding 20 R_J. Thus the Connerney model, particularly the analytical approximations discussed in the Appendix to Connerney et al. (1981), will be utilized to describe the external field. In a combined model we write

$$\bar{B} = \bar{B}_i + \bar{b}$$

where $\vec{B}$ is the total field, $\vec{b}$ the perturbation field due to external currents, and $\vec{B}_i$ is the internal field. $\vec{B}_i$ is derivable from a scalar potential (1) and $\vec{b}$ is computed as the curl of a vector potential $\vec{A}$ due entirely to external currents. The parameters of the model external current system and model internal field can then be simultaneously determined by inversion of the magnetic field data. In this paper we treat the parameters of the modeled external current system as fixed constants, determined by the V1, V2, and P10 encounters. Thus we assume at present that the near axis field due to external currents in the Jovian magnetosphere is time invariant, such that the model field fitted to the V1, V2 and P10 observations is appropriate to the P11 flyby as well. The magnetic field of the magnetopause and tail current systems is estimated to be only a few gammas in magnitude in the inner magnetosphere (Engle and Beard, 1980; Ness et al., 1979c) and is neglected in the computation of $\vec{b}$.

The perturbation field, $\vec{b}$, is computed using the approximate formulas given in the appendix to Connerney et al. (1981) for the near-axis region of the Jovian magnetosphere (in magnetic equatorial coordinates):

$$B_\rho = \left(\frac{\mu_o I_o}{2}\right) \frac{\rho}{2} [1/F_1 - 1/F_2]$$

and

$$B_z = \left(\frac{\mu_o I_o}{2}\right) [2D (z^2 + a^2)^{-1/2}$$

$$- \frac{\rho^2}{4} \left(\frac{z-D}{F_1^3} - \frac{z+D}{F_2^3}\right) - 2D(z^2 + b^2)^{-1/2}]$$

where

$$F_1 = [(z-D)^2 + a^2]^{1/2}$$

$$F_2 = [(z+D)^2 + a^2]^{1/2}$$

ρ and z are the radial and vertical coordinates, D is the annular current sheet half-thickness, and a (b) is the inner (outer) radial extent of the current annulus. For the V1 sheet model used in this paper, we adopt $(\mu_o I_o/2)$

= 225, a = 5 R_J, b = 50 R_J, and D = 2.5 R_J, the resulting field quantities expressed in gammas. Magnetic field quantities in the usual System III (1965) coordinate system are obtained by the appropriate coordinate transformation. The magnetic field topology in the magnetic equatorial plane of the field due to the V1 model current is illustrated in Figure 1. The magnitude of the field due to the sheet currents at the origin is ~ 200γ.

GENERALIZED INVERSE THEORY

The analysis of a linear system of the type (5) is conveniently accomplished using the generalized inverse theory that has been successfully utilized in the last decade in a number of branches of geophysics (Jackson, 1972; Pedersen, 1977; Wiggins, 1972). Instead of proceeding directly with the linear system (5), however, we will present the methodology in a form applicable to non-linear problems, in anticipation of non-linear relationships between the observations and the model parameters. For example, field magnitude observations (obtained while the spacecraft traversed Jupiter's shadow and lost orientation information) are non-linear in the parameters of the usual spherical harmonic models. Vector field observations are non-linearly related to model parameters in the context of the kind of models suggested in the previous section. Indeed, should correlative observations be included in the inversion process, it is likely that they too will be non-linear in the model parameters.

We assume that the i-th observation, Y_i, is related to the model parameters by the function $F_i(x_j)$. The functions $F_i(x_j)$ may be expanded in a Taylor series about some initial parameter set, x_j^o.

$$Y_i = F_i(X_j^o) + \frac{\partial F_i}{\partial X_j}\Big|_{X_j^o} \Delta X_j + \ldots$$

Neglecting all but terms of order 1, and letting $\Delta Y_i = Y_i - F_i(X_j^o)$,

$$\Delta Y_i = \left. \frac{\partial F_i}{\partial X_j} \right|_{X_j{}^o} \Delta X_j$$

which has the same form as the matrix equation

$$\bar{Y} = \bar{A} \bar{X} \tag{5}$$

If we let the column vector $\bar{Y}$ represent the model residuals (observed minus modeled field), the vector $\bar{X}$ represent the parameter corrections required to bring the model into closer agreement with the data, and the $\bar{A}$ matrix, a matrix of partial derivatives of the model field with respect to the model parameters, i.e.,

$$\bar{A} \equiv \begin{bmatrix} \dfrac{\partial F_1}{\partial X_1} & \cdots & \dfrac{\partial F_1}{\partial X_M} \\ \dfrac{\partial F_N}{\partial X_1} & \cdots & \dfrac{\partial F_N}{\partial X_M} \end{bmatrix}$$

We will proceed with (5) with the understanding that non-linear problems are accommodated by considering them to be locally linear and iterating to a final solution.

The matrix formulation of the generalized inverse method utilizes the singular value decomposition of Lanczos (Lanczos, 1961) to rewrite (5) as

$$\bar{Y} = \bar{U} \bar{\Lambda} \bar{V}^T \bar{X} \tag{6}$$

where $\bar{U}$ is an N x M matrix consisting of the M orthonormalized eigenvectors associated with the M largest eigenvalues of $\bar{A}\bar{A}^T$, $\bar{V}$ is the M x M matrix consisting of the orthonormalized eigenvectors of $\bar{A}^T\bar{A}$ as columns, and $\bar{\Lambda}$ is an M x M diagonal matrix consisting of the eigenvalues, λ_i, of $\bar{A}^T\bar{A}$. The $\bar{\Lambda}$ matrix is by convention assembled with the largest λ_i in the upper left, all elements positive and in order $\lambda_1 > \lambda_2 > \dots \lambda_M$, i.e.,

$$\bar{\Lambda} = \begin{bmatrix} \lambda_1 & o & \ldots & o \\ o & \lambda_2 & & \\ & & & \\ o & & & \lambda_M \end{bmatrix}$$

Operating on the left with U^T, we write

$$(\bar{U}^T \bar{Y}) = \bar{\Lambda}(\bar{V}^T \bar{X}) \tag{7}$$

Since $\bar{\Lambda}$ is an M x M diagonal matrix (7) can be regarded as M independent equations relating 'eigendata' (on the left), through the eigenvalues λ_i, to eigenvectors of parameter space, the linear combination of the original parameters $\bar{V}^T \bar{X}$. The solution to (5), that is, the parameter vector $\bar{X}$ minimizing in a least squares sense (Lanczos, 1961) the differences between the model and observations, is given by

$$\bar{X} = \bar{V} \overline{\bar{\Lambda}^{-1}} \bar{U}^T \bar{Y} \tag{8}$$

writing $\bar{\beta} = \bar{U}^T \bar{Y}$, the solution can be constructed by a summation over the orthonormalized $\bar{V}_i$ of parameter space:

$$\bar{X} = \sum_{i=1}^{M} (\beta_i / \lambda_i) \bar{V}_i \tag{9}$$

Considerable insight into the estimation problem can be obtained by an examination of (9). Assume that in the original statement of the problem (equation 5) the data are (by suitable transformation--see Jackson, 1972) normal random variables of zero mean and unit variance. In (9) the β_i are then of unit variance. The variance of the parameter vector (solution) is largely due to just a few of the λ_i's of the A matrix corresponding to the directions in the parameter space ($\bar{V}_i$'s) along which the solution is poorly determined. The singular value decomposition yields not only a method of constructing solutions but a characterization of both parameter and data space

11

as well.

We stated earlier that magnetic field observations along a flyby trajectory are insensitive to certain linear combination of parameters. One advantage of the singular value decomposition is that these parameter vectors which are poorly constrained by the available observations are explicitly identified, i.e., they are the eigenvectors associated with the small eigenvalues of $\bar{A}^T\bar{A}$. To illustrate this, we show in Figure 2a a surface isointensity contour map of a maliciously constructed, hypothetical Jovian magnetic field. Illustrated in Figure 2a is the surface expression of a particular combination of internal field parameters (eigenvector of parameter space) which leads to a virtually unobservable magnetic field along the Pioneer 11 trajectory, but a significant field elsewhere. Had Jupiter's internal field been so constructed, the Pioneer 11 fluxgate magnetometer would not have detected it. We have in this example assumed observations within 5 R_J at ∿ .5 minute intervals and a random noise component of .005 G everywhere; the parameter set for this example is just the appropriately scaled eigenvector associated with the minimum eigenvalue. In Figure 2b we show the surface isointensity contour map of an internal field which would be undetectable assuming measurements with a random noise component of 1% of the ambient Jovian field magnitude rather than a constant noise component as in 2a. Observations within 5 R_J of Jupiter at ∿ 1 minute intervals are assumed. Note that in this example the field magnitude is smaller but comparable to the previous example, and that the eigenvector is considerably different, reflecting a difference in information content in the two data sets.

The A matrix is a function of the trajectory, the model, and the transformation utilized to condition the data. If the model chosen is sufficiently accurate, or descriptive of the magnetic field environment, the Y_i (observed minus modeled field) will be of zero mean. Each observation, Y_i, and correspondingly, each row of the $\bar{A}$ matrix is divided by the estimated standard deviation of that observation, σ_i, such that the standardized variable Y_i/σ_i has a unit standard deviation. Thus the residual for each observation is scaled with the width of the population from which it was drawn, its expected error. For independent observations, the $\bar{A}$ matrix assumes the form

$$\bar{A}' = \begin{bmatrix} \dfrac{1}{\sigma_1} \dfrac{\partial F_1}{\partial X_1} & \cdots\cdots & \dfrac{1}{\sigma_N} \dfrac{\partial F_1}{\partial X_M} \\[2ex] \dfrac{1}{\sigma_N} \dfrac{\partial F_N}{\partial X_1} & \cdots\cdots & \dfrac{1}{\sigma_N} \dfrac{\partial F_N}{\partial X_M} \end{bmatrix} \tag{10}$$

corresponding to a least squares minimization of

$$(\bar{Y} - \bar{A}\ \bar{X})^T\ \bar{D}\ (\bar{Y} - \bar{A}\ \bar{X}) \tag{11}$$

where the matrix $\bar{D}$ is the diagonal matrix with elements $D_i = 1/\sigma_i^2$.

For data which are not statistically independent, the inverse covariance matrix of the observations replaces $\bar{D}$ in (11) (Jackson, 1972). In either case the choice of weights relates to the statistics of the noise on the data, and, by modification of the A matrix (10), alters not only the final model but the orthogonalization of data and parameter space as well. Thus care must be taken to insure that the weights chosen reflect some real knowledge of the noise statistics of the data.

We have thus far assumed that the M eigenvalues, λ_i, of the matrix $\bar{A}^T\bar{A}$ are non-zero, in which case (9) represents the classical least squares solution. The Lanczos inverse also leads to a solution when only K of the M eigenvalues are non-zero. The non-zero λ_i are arranged in the diagonal matrix $\bar{\Lambda}$ as before with λ_i, $i > K = 0$. Equation (9) becomes

$$\bar{X}(K) = \sum_{i=1}^{K}\ (\beta_i/\lambda_i)\ \bar{V}_i \tag{12}$$

i.e., only the eigenvectors corresponding to non-zero eigenvalues are allowed in the solution. Those parameter combinations which, by (6), do not contribute to the observations are ignored in the construction of the solution. The minimum length solution (12) is unique in the space spanned by the K eigenvectors V_i, $i = 1, K$, and has no projection along the remaining M-K eigenvectors (corresponding to the zero eigenvalues) which define the region

13

of parameter space that is inaccessible to the present linear system. This inaccessibility reflectes a basic lack of information inherent in the available observations. The unavoidable consequence of such a deficiency is a lack of parameter resolution, that is, the existence of linear combinations of parameters (V_i, i = K+1 ... M) which may be added to the solution of the linear system without change to the model response.

Eigenvalues which are non-zero but small lead to a similar loss of resolution when noise on the data is considered. The projection of the solution vector onto the V_i corresponding to the large λ_i will be well constrained; the projection onto the V_i associated with the small λ_i will be relatively poorly constrained, by virtue of the factor (β_i/λ_i) in (12).

Errors in the parameters resulting from noise upon the observations will appear predominently in linear combinations corresponding to the poorly determined eigenvectors. A vivid and perhaps more familiar example of this effect occurs in the geomagnetic field models derived from scalar observations. Stern and Bredekamp (1975) have shown that errors in field models derived from scalar data are enhanced for certain sequences of terms, first derived by Backus (1970). This 'Backus effect', subsequently observed (Stern et al., 1981) in models derived from Magsat observations, suggests the near-singular nature of the A matrix for this problem, and the presence of eigenvectors (related to the Backus series) which have small associated eigenvalues. Again assuming the data have been transformed such that the Y_i are statistically independent and of unit variance, the variance of the jth model parameter is

$$S^2_j (K) = \sum_{i=1}^{K \leq M} \frac{V_{j,i}^2}{\lambda_i} \qquad (13)$$

In constructing a solution vector, we are free to restrict the solution to K < M eigenvectors, reducing the parameter variance to an acceptable level. In so doing one avoids a large contribution to the parameters due entirely to a small noise component on the data, at the expense of an unavoidable loss of model parameter resolution.

Parameter resolution is conveniently described by the resolution matrix, R, (e.g., Jackson, 1972) relating the K eigenvector parameter estimate $\bar{X}(K)$ to a solution of the linear system (5),

$$\bar{X}(K) = \bar{V} \; \bar{\Lambda}_K^{-1} \; \bar{U}^T \; \bar{Y}$$

$$= \bar{V} \; \bar{\Lambda}_K^{-1} \; \bar{U}^T \; \bar{U} \; \bar{\Lambda} \; \bar{V}^T \; \bar{X}$$

$$= \bar{V}_K \; \bar{V}_K^T \; \bar{X}$$

$$R \equiv \bar{V}_K \; \bar{V}_K^T$$

The subscript K to a matrix denotes the matrix obtained by setting each column i for i > K of the original matrix to zero. An element $\bar{X}_i(K)$ of the estimated solution is the convolution of the ith row of the resolution matrix with a solution of (5). For K = M, the R matrix is the identity matrix; as fewer eigenvectors are admitted in the construction of the solution, the R matrix off-diagonal elements grow at the expense of the diagonal elements, reflecting a loss of parameter resolution. An example illustrating the trade-off between parameter standard deviation and resolution is given in Figure 3. In this example we assume an internal spherical harmonic field model of order 3 and 500 vector magnetic field observations along the Pioneer 11 trajectory within 5 R_J of Jupiter, the observations including a noise component with .005 G standard deviation. The RMS model residuals, g_1^0 parameter resolution (diagonal element of R) and the g_1^0 parameter standard deviation are shown as a function of the number of eigenvectors admitted in the construction of a solution. The very modest improvement in model fit (RMS) attained by using the last two eigenvectors is accompanied by a large increase in parameter standard deviation and only a small gain (2%) in parameter resolution. An estimate for g_1^0 of 4.35 G, based on the 13 ev fit, may be more appropriate than the estimate of 4.18 G resulting from the 15 ev solution. With 13 ev, the off-diagonal terms of the resolution matrix are sufficiently small that 'leakage' from the higher order parameters (which are presumably small in magnitude) into the g_1^0 estimate should not be important, i.e., g_1^0 is expected to be adequately resolved at R_{11} = .98.

The advantages of obtaining additional magnetic field information far removed from the observations available along the flyby trajectory can be understood by considering only the poorly determined parameter vectors. Such information may include the correlative observations referred to earlier as well as additional in situ magnetic field observations. The additional observations will in general be in regions where the poorly determined eigenvectors lead to relatively large fields (e.g., Figure 2). These new observations effectively limit the range accessible to the previously poorly determined eigenvectors, acting as a constraint on the solutions. This can be quantitatively explored by forming a combined system of all the observations (e.g., equation 10) and comparing the new eignevalues with the old, or in an approximate way (Jackson, 1972) by estimating the (larger) eigenvalues of an augmented A matrix of N + 1 rows. The potential benefits in terms of improved model parameter variance and resolution are great since they depend critically upon the minimum eigenvalue.

To define the entire range of values a parameter may assume, we use the concept of an extreme parameter set as developed by Johansen (1977). Because of correlations between the parameters, the extreme value of any parameter is achieved for a specific parameter vector—its extreme parameter set. This represents the direction in parameter space along which the model response (RMS change) is minimized for a change in a specified parameter. This direction is found by considering the change in the model response, ΔQ, due to an excursion, $\bar{\epsilon}$, in parameter space from the model minimum

$$\Delta Q = \bar{\epsilon}^T \; V \; \bar{\Lambda}^{-2} \; V^T \; \bar{\epsilon} \tag{14}$$

In the coordinate system defined by the eigenvectors V_i, ΔQ is given by

$$\Delta Q = \bar{\epsilon}'^T \; \bar{\Lambda}^{-2} \; \bar{\epsilon}' \tag{15}$$

describing an M dimensional hyperellipsoid with axes parallel to the V_i's of length $\alpha \; 1/\lambda_i$. The extreme parameter set associated with the extreme values of the ith parameter is determined by requiring the gradient of the error surface to have only a component along the ith parameter.

$$\nabla \bar{\Lambda}^2 \nabla^T E_i = s\bar{a}_i$$

where $\bar{a}_i$ is the column vector with the ith element equal to one and all others zero, resulting in

$$E_i = S \bar{V} \overline{\Lambda^{-2}} \bar{V}^T \bar{a}_i \qquad (16)$$

where S is a constant and E_i is the extreme parameter set for the ith parameter. Any linear combination of the model parameters may be extremized in this fashion. In actual practice one perturbs the solution in the direction given by (16) until ΔQ appropriate to a specified significance level is achieved to find the magnitude of the extreme parameter sets, as suggested by Johansen (1977). This procedure requires that the problem be sufficiently linear in the neighborhood of the solution such that the basis vectors of parameter space ($\bar{V}_i$'s) are not appreciably altered in the process. The problems considered here are sufficently linear that we may use for S the value obtained from the linear approximation, resulting in

$$E_i = \bar{V} \overline{\Lambda^{-2}} \bar{V}^T \bar{a}_i / || \overline{\Lambda^{-1}} \bar{V}^T \bar{a}_i || \qquad (17)$$

for $\Delta Q = 1$, corresponding to a 68% confidence limit.

One additional practical consideration relating to the non-linearity of the problem has to do with the method (9) of constructing solutions at each iteration. If the A matrix is close to being ill-conditioned in the sense that some of the λ_i are very small, the solution vector will require a large step in parameter space which may well be greater than the region in which the linearization is appropriate. The iterative process may then diverge unless some method of limiting the iterative step size is employed. In such cases the stability of the iterative procedure is improved by limiting the step size (noteably in the directions corresponding to the small eigenvalues) by using (e.g., Lawson and Hanson, 1974, Chapter 25)

$$\bar{X} = \sum_{i=1}^{K} \frac{\beta_i \lambda_i}{(\lambda_i^2 + \alpha^2)} \bar{V} \qquad (18)$$

17

where α is chosen approximately equal to the smallest eigenvalue included in the inversion. This technique (known as Marquardt's algorithm) is invoked only as convergence problems arise and is quite unnecessary in the context of the present nearly-linear problems considered here.

APPLICATION TO PIONEER 11 OBSERVATIONS

The Pioneer 11 spacecraft had onboard two magnetic field experiments (Smith et al., 1976; Acuna and Ness, 1976), each of which recorded the magnetic field along the Pioneer 11 trajectory. The vector helium magnetometer (VHM) has been described by Smith et al. (1975) as accurate at the 1% level (at low field values) whereas the high field fluxgate (FGM) is essentially a constant noise instrument with a quantization uncertainty of .006 gauss (Acuna and Ness, 1975). The high field instrument would be expected to provide a better estimate of the Jovian field near close approach ($|B| \sim 1.13$ Gauss at the inbound occulation) while the vector helium magnetometer would out perform the fluxgate in a low field environment. In either case the random noise component assumed in what follows is a sum of all noise sources, including, for example, instrumentation noise and local magnetospheric noise. A single least squares fit to the combined data sets, each observation appropriately weighted as discussed in the previous section, would result in the optimal model. Unfortunately, the two data sets are incompatible in the sense that the systematic differences in the observed field as measured by the two instruments are larger than expected on the basis of the instrument descriptions. This is illustrated in Figure 4, which shows the differences between the VHM and FGM measurement, for each component of the field during encounter as a percentage of the total field magnitude. Rather than produce a model which fits neither set of data, we will of necessity continue the practice of considering each data set independently. Resolution of the differences between the two data sets is beyond the scope of the present work.

The FGM observations have been analyzed by Acuna and Ness (1976a,b) in the traditional least squares fit to a spherical harmonic expansion of order 3

18

including internal terms only. They obtained the GSFC O_4 internal field model as the unweighted least squares solution to 685 vector observations at radial distances of $R < 6 R_J$. Details of their analysis are given in Acuna and Ness (1976b). We will first present the results of a similar analysis, assuming an expansion of internal harmonics to order 3, but within the framework of the generalized inverse methodology. A model explicitly including the effects of the field due to external currents will then be considered.

Our FGM data set consists of 499 vector observations obtained approximately every 35 seconds along the Pioneer 11 trajectory within 5 R_J radial distance, and 20 field magnitude observations obtained near closest approach when the orientation of the spacecraft is uncertain. Inclusion of the magnitude observations along this part of the trajectory increases the information content of the data set at the expense of introducing some non-linearity in the estimation problem and requiring an iterative solution. Since the FGM is essentially a constant noise instrument (Acuna and Ness, 1975), and the FGM observations are limited by instrument noise, we choose for each observation equal weights (Eqn. 10) of $\sigma_i = .005$ Gauss. The use of equal weights introduces only a scale factor as compared with an unweighted least squares and does not effect the orthogonalization of parameter space or the final model. Assuming as a model a Schmidt normalized spherical harmonic expansion of order n = 3 (internal terms only) we find after two iterations a 15 eigenvector fit (Eq. 9) very similar to the GSFC O_4 model, differences between the two solutions due only to a difference in observations used. The salient features of the singular value decomposition are illustrated in Figure 5, at the final iteration. In this figure the eigenvalues of the A matrix, and the associated eigenvectors of parameter space are listed, in addition to the solution vector, parameter standard deviations (Eq. 13) and extreme parameter sets (Eq. 16). A diagnostic parameter 'lin' is also indicated: this is the cosine of the angle between the parameter vector and the local normal to the error surface. A change in the value of an individual parameter with lin $\approx$ 1 results in a comparatively large model response (RMS increase) since that parameter vector is nearly perpendicular to the error surface, that is, it is oriented in the direction of the maximum model response (RMS change). The weighted RMS residual is computed at each iteration assuming internal consistency (Birge, 1932)

$$s^2_{INT} = \frac{N}{\sum\limits^N 1/\sigma_i^2} \; ,$$

essentially a prediction of the probable error based on propagation of errors, and also assuming external consistency

$$s^2_{EXT} = \frac{\sum\limits^N (\epsilon_i/\sigma_i)^2}{\sum\limits^N 1/\sigma_i^2}$$

based on the realized differences, ϵ_i. A comparison of these two estimates is often useful in identifying the presence of systematic effects in the data.

The eigenvalues for this system range from ∿650 to ∿10. The classical measure of the condition, or stability, of a linear system is the 'condition number', ν, defined as the ratio of the largest and smallest eigenvalue (Lanczos, 1971),

$$\nu = \frac{\lambda_1}{\lambda_M}$$

or sometimes the square root of the above. In the present example, a 'condition number' of $\nu \approx 65$ is interpreted in the following way: errors in the 15th generalized parameter (15th eigenvector) can be expected to be ∿65 times larger in magnitude than errors in the 1st generalized parameter. The 'condition number' is thus a useful tool in diagnosing the need for a singular value analysis, but it cannot address individual parameter errors or resolution, or correlations among the model parameters.

Inspection of the eignevectors associated with the eigenvalues of the A matrix is useful in visualizing the characteristics of the problem solution. For example, in Figure 5, the eigenvectors associate with the small eigenvalues are the linear parameter combinations which are poorly constrained by the observations. The parameter with the smallest absolute error ($J = 2$; parameter $g_1^{\,1}$) has only small components among the last (poorly determined) 5 eigenvectors, that is, it is well approximated by a linear combination of the first (well determined) 10 eigenvectors. Conversely, the parameters with the

largest absolute errors ($J = 11$, g_3^2, and $J = 13$, h_3^1) are those which are heavily represented in the last few eigenvectors. Furthermore, these two parameters are equally represented in the 15th eigenvector but with opposite signs, indicating a strong negative correlation between these two parameters. A change in the parameter g_3^2 will most likely be accompanied by a nearly equal and opposite change in the parameter h_3^1. A similar relationship exists between the parameters g_3^1 ($J = 10$) and g_3^3 ($J = 12$), as evidenced in the 14th eigenvector.

The extreme parameter sets are listed in Figure 5 for each parameter, computed using (16). These are the parameter combinations which may be added to or subtracted from the optimal solution to achieve the extreme values of each individual parameter. The error surface chosen here is $\Delta Q = 1$ corresponding to a 68% confidence limit.

A useful illustration for the purpose of emphasizing the differences between internal field models is a surface isointensity contour map such as that in Figure 2a. Figure 2a, the 'undetectable planet' was constructed by selecting the internal field coefficients to be proportional to the 15th eigenvector, that combination of parameters to which the observations are least sensitive. It is perhaps more instructive to compare the surface isointensity contour map corresponding to the best fitting model (Figure 6) with the surface isointensity contour maps that result when this parameter vector is added to (Figure 7a) or subtracted from (Figure 7b) the least squares solution. These two extreme models lead to differences in the surface field magnitude of ~ 1 G.

While this example is representative of the differences in field topology and magnitude appropriate to the range of models consistent with the observations, it is by no means unique. Any linear combination of the poorly determined eigenvectors, consistent with the constraint (14) and some chosen significance level (ΔQ), can be added to the least squares solution with similar results. The surface isointensity contour map corresponding to the least squares 15 eigenvector solution, is practically identical to that of the GSFC O_4 model of Acuna and Ness (1976), reflecting only differences in the radial extent of observations included in the analysis and the inclusion of

additional magnitude observations near close approach. Thus, the model uncertainties illustrated in Figure 7 can also be regarded as typical of the O_4 model.

For some applications a model constructed of only 13 eigenvectors, ignoring the last two (poorly determined) eigenvectors, may be preferable to the 15 eigenvector solution. In Figure 3 it is clear that the 15 eigenvector fit is only marginally better than the 13 eigenvector fit in terms of the RMS of the residuals (although the 14th and 15th parameter vectors are statistically significant, in that β_{14} and $\beta_{15} > 1$). The loss in parameter resolution that results in constructing the solution with only the first 13 eigenvectors is illustrated in Figure 8, which lists the resolution matrix as well as the quantities discussed in the context of the 15 eigenvector fit. All of the low order terms ($n = 1$, $n = 2$) are well resolved, since the corresponding diagonal elements of the resolution matrix are near unity. Additionally, the g_3^0 term ($J = 9$) is well resolved, and the h_3^3 term ($J = 15$) somewhat less so. The remaining 3rd order terms are rather poorly resolved. The surface isointensity map of this model field, illustrated in Figure 9, is more dipolar than that of the 15 eigenvector fit as a result of the concentration of higher order parameters in the unused eigenvectors. While the 13 eigenvector model may provide a better estimate of the well resolved parameters, it is unique only in a subset of parameter space. We are free to add linear combinations of the excluded eigenvectors to the solution, subject to some maximum allowable RMS increase corresponding to a chosen significance level.

Two observations remaining to the model residuals for the FGM data set are of importance in regard to the significance level corresponding to the choice of $\Delta Q = 1$. The first is that the RMS of the residuals, ~ 500 γ, is largely due to the quantization step size of the instrument; the true instrumentation noise is a fraction of that. The second is that the quantization noise is not random, rather, it exhibits a positive correlation at small lags and a negative correlation at larger lags. The correlation length is several samples (minutes) at large radial distances (5 R_J) where the field is comparatively small. At small radial distances the correlation vanishes. The quantization errors, however, do not seriously affect the model, as they are as often positive as negative. In constructing solutions

22

(9) only the quantity $\bar{\beta} = U^T \bar{\gamma}$ is important, and the sum over the quantization errors is likely to be small since each positive residual is paired with a nearly equal negative residual in the immediate vicinity. The quantization errors contribute substantially to the RMS of the residuals, but not appreciably to the model misfit. Thus the correlation among the residuals, effectively decreasing the number of independent observations, is largely offset by the decrease in the estimated noise upon the data (disregarding the quantization 'noise'). For this reason we regard the choice of σ = 500 γ, corresponding to $\backsim$ 68% confidence level of a Gaussian distribution as a conservative estimate.

We have demonstrated that a sizeable parameter vector can be found (e.g., Figs. 2a, 2b) which leads to a small field along the Pioneer 11 trajectory. In much the same way a small field (systematic 'error') along the Pioneer 11 trajectory can lead to a large error in the estimated parameters. The magnetic field of the large scale azimuthal currents produce a large ($\backsim$200γ) correlated 'error' along the entire Pioneer 11 trajectory under consideration (Conne.ney et al., 1981). This 'error' contributes substantially to $\bar{\beta} = U^T \bar{\gamma}$ due to the large positive correlation (no cancellation) and thus results in a significant bias in the derived internal field models. The best way to remove such a bias is to include explicitly the magnetic field produced by these currents in the physical model chosen to represent the observations. A 15 eigenvector fit to the FGM observations, assuming a N = 3 internal spherical harmonic expansion and the V1 model external field, results in a modest RMS decrease to 492 γ but a significant change in many of the model parameters (Table 1). Comparison of the surface isointensity contour map of this model field (Figure 10) with that of the earlier 15 eigenvector model (Figure 6) indicates surface field magnitude errors of $\backsim$1 Gauss result from neglect of the external field in the earlier model. Differences in the internal field parameters resulting from inclusion of the sheet field are as large as $\backsim$ .12 G (Table 1) and often larger than the corresponding parameter standard deviations. Thus the presence of an unmodeled field of external origin is at least as important as the noise on the data in this examaple. Since no additional free parameters have been introduced (the parameters of the current sheet regarded as fixed, determined by the more advantageous Pioneer 10 and Voyager flybys) the singular value decomposition remains unchanged. A

formulation of this problem in which the sheet parameters are treated as variables would show more clearly the interdependence of the internal coefficients and the current sheet parameters.

The VHM observations have been analyzed (Smith et al., 1976; Davis and Smith, 1976; see also Smith and Gulkis, 1979) in the traditional least squares fit to a spherical harmonic expansion. Noteable differences in their analysis include a larger radial range of observations used ($r < 8 R_J$), the use of external spherical harmonics in the expansion (2), and the use of a r^α weighting scheme whereby all observations are weighted with some power of the radial distance of the observation. For reasons discussed in Davis and Smith (1976) this group prefers a $r^{3/2}$ weighting of each observation. In addition, they use (Davis and Smith, 1976) ~5 minute averaged values of the observed field along the trajectory in their analysis.

Our VHM data set consists of 324 vector ($\sim$ 1 minute averages) observations within $R = 5 R_J$ of Jupiter as obtained from the National Space Science Data Center at Goddard Space Flight Center. In contrast to the uniform weighting appropriate to the FGM observations, we adopt for the VHM observations weights proportional to the local field magnitude, $\sigma_i = .01 |B|$. The constant of proportionality adopted here (.01) enters only as a scale factor in the error analysis. This particular weighting, appropriate for observations with a noise component of 1% of the local $|B|$, results in a more heavily weighted (in r) system than any of the r^α schemes proposed by Davis and Smith (1976). (The weights, w_i, defined by Smith et al. (1976) and Davis and Smith (1976) appear linearly in their formulation of the least squares problem. Therefore these w_i must be compared to the square of the weights ($1/\sigma_i$) appearing in this work.) The resulting model (listed in Table 1) leads to a surface isointensity contour map, illustrated in Figure 11, that is much more similar to that of the FGM (or GSFC O_4) model than previous analyses of these data (using $r^{3/2}$ weights) would suggest. The choice of weights proportional to $|B|$ affects not only the final model but the orthogonalization of parameter space as is illustrated in Figure 12. We have assumed in this example a model field of internal terms to order 3 so that the VHM and FGM inversions can be directly compared. Comparing the eigenvalues of the two inversions, we note that the FGM observations lead to a slightly better

24

determination of some eigenvectors and a poorer determination of others. Yet individual parameters would be better determined by the VHM inversion since they require a summation over many eigenvectors. The 'lin' diagnostic parameter demonstrates that all of the dipole parameters in the VHM inversion lie closer to the eigenvectors of parameter space in this problem and therefore are more easily estimated independently of the other parameters. A detailed study of the remaining features of this singular value decomposition is similar to the FGM example and thus will not be repeated; instead we will address an additional concern of systematic errors present in the VHM model residuals.

The fact that the model residuals are characterized by an extremely large correlation length precludes any attempt to quantify the parameter errors. For this reason the extreme parameter sets have been omitted and the quoted parameter standard deviations are to be disregarded. These systematic errors include the presence of an unmodeled external field, which we shall return to shortly, and systematic errors associated with instrumental range changing and other effects (see Davis and Smith, 1976, Figure 1 and accompaning discussion). While these effects are only as large as $\sim$ .5 or 1% of the total field they do dominate the observed residuals. Another systematic effect in previous analyses of these data involves the use of 5 minute averages of the field as instanteous values. Near close approach, the 5 minute averaged field differs by as much as 0.6% from the instantaneous field at the midpoint of the data averaging interval (which is used as the model field). Since this effect is comparable in size to the observed residuals it seems appropriate to use 1 minute averages instead or compute the model response as the averaged field over the measurement interval. We have chosen to use $\sim$1 minute averages as supplied by the NSSDC for computational convenience.

Inclusion of the magnetic field contribution due to the external currents in the analysis of the VHM observations leads to a much improved fit to the observations. The resulting parameter set, listed in Table 1, leads to a surface isointensity contour map (Figure 13) that still resembles the previous map but differs in field magnitude by $\sim$1 G at the surface. Differences in the internal field parameters are as large as $\sim$ .2 G, occurring predominently in the quadrapole and octopole terms. A more dramatic decrease in the RMS of the

residuals from 93 γ to 57 γ results from the use of the V1 current sheet model
in the inversion, in contrast to the relatively modest improvement (504 γ to
492 γ) noted in the FGM fit. It is worthwhile to note again that this
improvement in the RMS residuals is not gained at the expense of additional
free parameters, i.e., the sheet field is regarded as a known (based on the
other Pioneer 1C and Voyager 1, 2 flybys) quantity. A relatively modest
further improvement in the RMS of the residuals (to 56γ) is obtained by
assuming either a closer inner radius of 4 R_J rather than 5 as in the V1
model, or a constant $\mu_o I_o / 2 = 250$ rather than 225 as in the V1 model. Again,
a simultaneous inversion of the internal and external field parameters would
yield more information, but must await further analysis of the Voyager
observations. The kind of correlations existing between internal and external
field parameters that would be evident in a singular value decomposition of a
combined internal/external system are already implied in the present analysis.
Note that the internal field parameters have been able to 'absorb' most of the
external field, which averages ~200 γ along the trajectory. The ability of
the external field to partially masquerade as internal coefficients, leading
to the large parameter changes indicated in Table 1, portends such an
interplay of internal and external field parameters.

DISCUSSION

The internal Jovian field models presented here differ substantially from
the models of Acuna and Ness (1976) and Smith et al. (1976). In the first
case the difference arises almost entirely out of a consideration of the
fields of external origin, while in the second both the weights applied to the
observations and the inclusion of the fields of external origin contribute to
the difference. The resulting models are found to be more similar than
previously thought. The large differences in the models of Table 1, based on
the VHM observations, and the models of Smith et al. (1976) bears witness to
the effects of the weighting scheme utilized to condition the observations,
and to the increased importance of external fields in this data set. Indeed,
the weights utilized in this paper as appropriate to the VHM observations have
in fact made the model more sensitive to small fields at greater distances and
elevated the importance of unmodeled external fields.

The differences between the internal field models advocated here (GSFC 15 evs and JPL 15 evs, outlined in Table 1) and previous models are more readily apparent in Figures 14 and 15. In Figure 14 we compare the GSFC 15 evs and O_4 models on the (oblate) Jovian surface by contouring the difference in field direction and the normalized difference in field magnitude resulting from each model. These differences are greatest in the northern hemisphere, where the local field angle differs by up to 4° and the local field magnitude differs by as much as 8%. In Figure 15 the same comparison is made between the JPL 15 evs model and the SHA 23 model. Here again the differences appear greatest in the northern hemisphere, where the local field direction differs by up to 30° and the local field magnitude differs by as much as 50%. A similar comparison between the JPL 15 evs and the more recent P11A model (Smith et al., 1976) leads to difference contours much like those illustrated in Figure 15 but with maximum differences of 18° in field angle and 20% in field magnitude. The P11A model is a fit to observations obtained by both Pioneer 10 and 11, however, and therefore is not directly comparable to the JPL 15 evs model. But the inclusion of additional observations along another trajectory in the P11A model fit apparently results in an internal field model that more closely resembles the JPL 15 evs model presented here.

The generalized inverse technique described here should prove valuable not only in the estimation of planetary magneic fields and the study of non-uniqueness problems encountered in geomagnetic models based on scalar observations (e.g., Stern et al., 1981), but in a variety of other multivariate problems as well. The methodology has been widely used in related geophysical disciplines in the past decade and has proven to be a powerful analysis tool. Indeed, some (e.g., Wiggins, 1972) consider multivariate inversion studies without such resolution analyses to be incomplete at best, and often misleading. In such cases the magnitude of the condition number of the (appropriately weighted) matrix to be inverted can be diagnostic of the need for a singular value decomposition.

The kind of model advocated here, combining an internal spherical harmonic expansion with an explicit model of the field due to external current systems, is regarded as essential to understanding and integrating the magnetic field observations of each of the spacecraft that have thus far

encountered Jupiter. Perhaps one model will ultimately enable meaningful
comparisons of the various flybys and a more detailed description of the inner
magnetosphere of Jupiter. Further progress can be expected from analysis of
the Voyager observations and also possibly from further analysis of the
Pioneer 10 and 11 observations. At the present level of analysis, the small
instrumental and other systematic effects present in the VHM observations are
the most important remaining source of errors. For the purpose of eliminating
or reducing these effects (and quantization errors in the FGM data as well)
further analysis, conducted in payload coordinates, would be extremely useful.
Analysis of the data in payload coordinates, while cumbersome, enables the
modeling of quantization errors, axis non-orthogonality, and range sensitivity
or gain errors. Such an analysis is not currently possible with the reduced
data available at the NSSDC.

ACKNOWLEDGMENTS

REFERENCES

Acuna, M. H., and N. F. Ness, The Pioneer XI high field fluxgate magnetometer, Space Sci. Inst., 1, 177, 1975.

Acuna, M. H., and N. F. Ness, The main magnetic field of Jupiter, J. Geophys. Res., 81, 2917, 1976a.

Acuna, M. H., and N. F. Ness, The main magnetic field of Jupiter, in Magnetospheric Particles and Fields, ed. B. M. McCormac, 311-323, D. Reidel Publ. Co., Dordrecht, Holland, 1976b.

Acuna, M. H., N. F. Ness, and J. E. P. Connerney, The magnetic field of Saturn: Further studies of the Pioneer 11 observations, J. Geophys. Res., 85, 5675, 1981.

Backus, G. E., Non-uniqueness of the external geomagnetic field determined by surface intensity measurement, J. Geophys. Res., 75, 6339, 1970.

Barish, F. D., and R. A. Smith, An analytical model of the Jovian magnetosphere, Geophys. Res. Lett., 2, 269, 1975.

Beard, D. B., and D. J. Jackson, The Jovian magnetic field and magnetosphere shape, J. Geophys. Res., 81, 3399, 1976.

Birmingham, T. J., Jovian magnetic models and the polarization angle of Jovian decimetric radiation, submitted to Ap. J., 1980.

Birge, R. T., The calculation of errors by the method of least squares, Phys. Rev., 40, 207, 1932.

Chapman, S., and J. Bartels, Geomagnetism, Volume 2: The analysis and synthesis of geomagnetic data, Oxford Univ. Press, London, England, 1940.

Connerney, J. E. P., M. H. Acuna, and N. F. Ness, Modeling the Jovian current sheet and inner magnetosphere, J. Geophys. Res., in press, 1981.

29

Davis, L., and E. J. Smith, The Jovian magnetosphere and magnetopause, in
Magnetospheric Particles and Fields, ed. B. M. McCormac, 301-310, D.
Reidel Pbul. Co., Dordrecht, Holland, 1976.

de Pater, I., A comparison of radio data and model calculations of Jupiter's
synchrotron radiation: II. E. W. asymmetry in the radiation belts as a
function of Jovian latitude, J. Geophys. Res., (submitted) 1981.

Engle, I. M., and D. B. Beard, Idealized Jovian magnetosphere shape and field,
J. Geophys. Res., 85, 579, 1980.

Goertz, C. K., D. E. Jones, B. A. Randall, E. J. Smith, and M. F. Thomsen,
Evidence for open field lines in Jupiter's magnetosphere, J. Geophys.
Res., 81, 3393, 1976.

Goldstein, M. L., A. Eviatar, and J. R. Thieman, A beaming model of the
Io-independent Jovian decameter radiation based on multipole models of
the Jovian magnetic field, Ap. J., 229, 1186, 1979.

Hide, R., and S. R. C. Malin, On the size of Jupiter's electrically conducting
fluid core, Nature, 280, 42, 1979.

Jackson, D. D., Interpretation of inaccurate, insufficient, and inconsistent
data, Geophys. J. R. Astr. Soc., 28, 97, 1972.

Johansen, H. K., A man/computer interpretation system for resistivity
soundings over a horizontally stratified earth, Geophy. Prosp., 25, 667,
1977.

Jones, D. E., J. G. Melville, II, and M. L. Blake, Modeling Jupiter's current
disc: Pioneer 10 outbound, J. Geophys. Res., 85, 3329, 1980.

Lanczos, C., Linear differential operations, 564 pp., D. Van Nostrand Company,
Ltd., London, England, 1971.

Lawson, C. L., and R. J. Hanson, Solving least squares problems, 340 pp., Prentice-Hall, Inc., Englewood Cliffs, N.J., 1974.

Ness, N. F., M. H. Acuna, R. P. Lepping, L. F. Burlaga, K. W. Behannon, and F. M. Neubauer, Magnetic field studies at Jupiter by Voyager 1: Preliminary results, Science, 204, 982, 1979a.

Ness, N. F., M.. H. Acuna, R. P. Lepping, L. F. Burlaga, K. W. Behannon, and F. M. Neubauer, Magnetic field studies at Jupiter by Voyager 2: Preliminary results, Science, 206, 966, 1979b.

Ness, N. F., M. H. Acuna, R. P. Lepping, K. W. Behannon, L. F. Burlaga, and F. M. Neubauer, Jupiter's magnetic tail observed by Voyager 1, Nature, 280, 799, 1979c.

Pedersen, L. B., Interpretation of potential field data: A generalized inverse approach, Geoph. Prosp., 25, 199, 1977.

Smith, E. J., L. Davis, Jr., D. E. Jones, P. J. Coleman, D. S. Colburn, P. Dyal, C. P. Sonnet, and A. M. A. Frandsen, The planetary magnetic field and magnetosphere of Jupiter: Pioneer 10, J. Geophys. Res., 79, 3501, 1974.

Smith, E. J., B. V. Connor, and G. T. Foster, Jr., Measuring the magnetic fields of Jupiter and the outer solar system, IEEE Trans. on Magnetics, MAG-11, 962-980, 1975.

Smith, E. J., and S. Gulkis, The magnetic field of Jupiter: A comparison of radio astronomy and spacecraft observations, Ann. Rev. Earth Planet Sci., 1, 385, 1979.

Smith, E. J., L. Davies, Jr., and D. E. Jones, Jupiter's magnetic field and magnetosphere, in Jupiter, The Giant Planet, ed. T. Gehrels, 788-829, 1976.

Stern, D. P., and J. H. Bredekamp, Error enhancement in geomagnetic models

derived from scalar data, <u>J. Geophys. Res</u>., <u>80</u>, 1776, 1975.

Stern, D. P., R. A. Langel, and G. D. Mead, Backus effect observed by Magsat,
  <u>Geophys. Res. Lett</u>., in press, 1981.

Van Allen, J. A., D. N. Baker, B. A. Randall, and D. D. Sentman, The
  magnetosphere of Jupiter as observed with Pioneer 10 1: Instrument and
  principal findings, <u>J. Geophys. Res</u>., <u>79</u>, 3559, 1974.

Wiggins, R. A., The general linear inverse problem: Implication of surface
  waves and free oscillations for earth structure, <u>Rev. Geophys. Space
  Phys</u>., <u>10</u>, 251, 1972.

FIGURE CAPTIONS

Figure 1. Magnetic field topology in the magnetic equatorial plane of the
field due to large scale azimuthal currents in the Jovian magnetosphere
(V1 model of Connerney et al., 1981). The current flows eastward in an
annulus 5 R_J thick extending from 5 to 50 R_J.

Figure 2. 'Invisible planet': Surface isointensity contour map of a Jovian
model magnetic field which would not have been detected by a magnetometer
on Pioneer 11 (a) (upper panel) assuming observations with a .005 G
random noise component; (b) (lower panel) with a noise component
proportional to the local field magnitude (see text). A dynamical
flattening of 1/15.4 is assumed in the determination of the surface
equipotential (all surface maps).

Figure 3. Pioneer 11 FGM inversion example illustrating the trade-off between
parameter resolution and parameter standard deviation of the main dipole
coefficient (g_1^0 term).

Figure 4. A comparison of the Pioneer 11 FGM and VHM measurements of the
Jovian magnetic field within 6 R_J. Quantization effects are evident at
large radial distances, but the systematic differences between the two
measurements are clearest near close approach.

Figure 5. Pioneer 11 FGM inversion example at the final (third) iteration.

Figure 6. Jovian surface isointensity contour map illustrating a 15
eigenvector solution using the Pioneer 11 FGM observations.

Figure 7a,b. Jovian surface isointensity contour maps obtained by perturbing
the FGM 15 ev solution by a parameter set (proportional to the 15th ev)
to which the observations are least sensitive. These maps illustrate the
differences in surface field magnitude appropriate to the range of
internal field models consistent with the observations.

Figure 8. Pioneer 11 FGM inversion example illustrating a 13 eigenvector

33

solution.

Figure 9. Jovian surface isointensity contour map of the 13 ev solution using
Pioneer 11 FGM observations.

Figure 10. Jovian surface isointensity contour map of the 15 ev solution
model, obtained from the Pioneer 11 FGM observations and a model magnetic
field in which external sources are explicitly included.

Figure 11. Jovian surface isointensity contour map of the 15 ev solution using
Pioneer 11 VHM observations.

Figure 12. Pioneer 11 VHM inversion example.

Figure 13. Jovian surface isointensity contour map of a 15 ev solution using
Pioneer 11 VHM observations and a model magnetic field in which external
sources are explicitly included.

Figure 14. Comparison of the GSFC 15 evs magnetic field model and the O_4
model at Jupiter's surface. In the upper panel the difference in field
direction (degrees) is contoured. In the bottom panel the normalized
difference in local field magnitude (percent) is contoured.

Figure 15. Comparison of the JPL 15 evs magnetic field model and the SHA 23
model, differences contoured as in Figure 14.

TABLE 1

J	COEFF	GSFC					JPL		SHA 23[B]	P11A[C]
		0_4[A]	15 EV	15 EVS	(2 σ)	13 EV	15 EV	15 EVS		
1	g_1^0	4.218	4.184	4.201	(.030)	4.352	4.064	4.068	4.092	4.144
2	g_1^1	-.664	-.647	-.657	(.019)	-.656	-.675	-.668	-.705	-.692
3	h_1^1	.264	.235	.258	(.024)	.341	.269	.243	.231	.234
4	g_2^0	-.203	-.210	-.211	(.023)	-.197	-.098	-.093	-.033	.038
5	g_2^1	-.735	-.737	-.686	(.039)	-.557	-.757	-.672	-.699	-.581
6	g_2^2	.513	.554	.509	(.048)	.267	.550	.502	.537	.442
7	h_2^1	-.469	-.499	-.461	(.037)	-.306	-.556	-.498	-.531	-.427
8	h_2^2	.088	.092	.110	(.037)	.187	.110	.119	.074	.134
9	g_3^0	-.233	-.223	-.186	(.060)	-.138	-.306	-.111	-.113	-.147
10	g_3^1	-.076	.019	-.002	(.083)	-.324*	-.333	-.316	-.585	-.502
11	g_3^2	.168	.220	.150	(.080)	-.176*	.249	.220	.283	.351
12	g_3^3	-.231	-.312	-.235	(.082)	.124*	-.350	-.250	.067	-.136
13	h_3^1	-.580	-.668	-.575	(.104)	-.053*	-.615	-.476	-.423	-.342
14	h_3^2	.487	.619	.512	(.108)	.083*	.465	.380	.120	.297
15	h_3^3	-.294	-.307	-.307	(.068)	-.311*	-.264	-.228	-.171	-.041

* $R_{jj} < .9$ (POORLY RESOLVED)

1965 SYSTEM III φ POSITIVE EAST

SCHMIDT NORMALIZED — SPHERICAL HARMONIC COEFFICIENTS, GAUSS

A. Acuna and Ness (1976); Rotated to 1965 System III
B. Smith et al. (1976); rotated to 1965 System III
C. Smith and Gulkis (1979); rotated to 1965 System III

FIELD GEOMETRY OF THE ANNULAR CURRENT SHEET
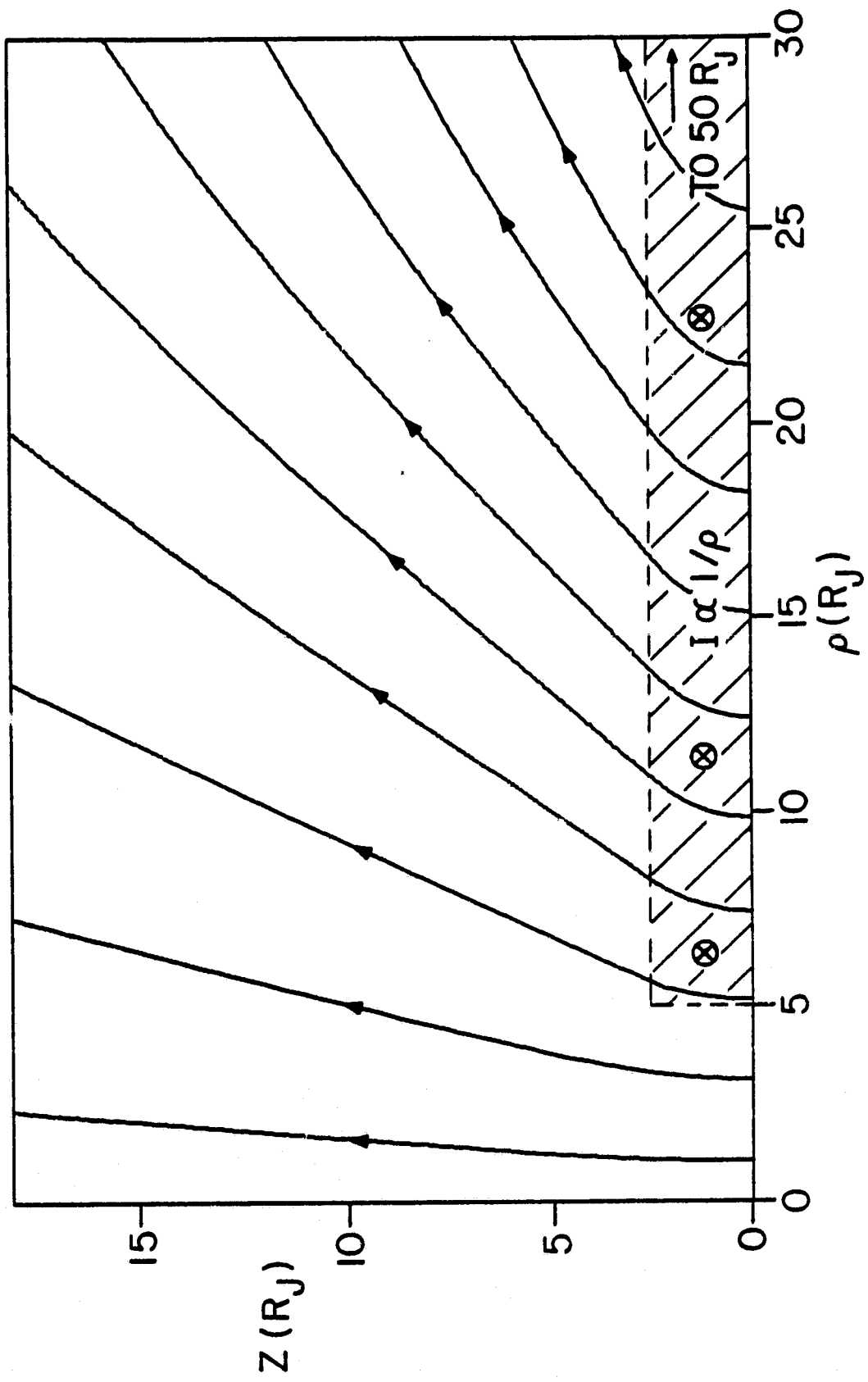
JOVIAN SURFACE ISOINTENSITY CONTOUR MAPS
P11 TRAJECTORY

PARAMETER RESOLUTION

RESOLUTION

STANDARD DEVIATION g_1^0

RMS (nT)

$g_1^0 G$
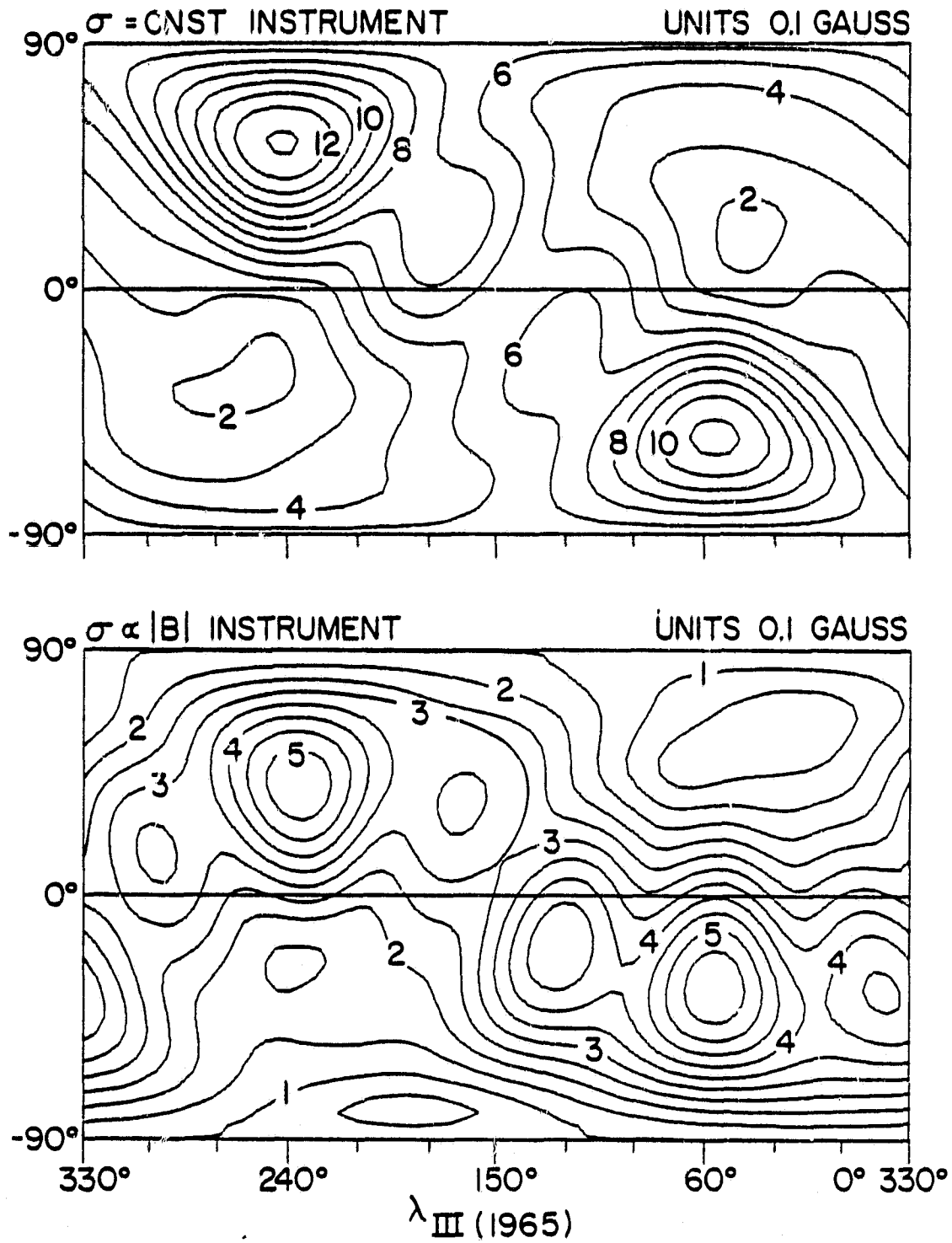
NUMBER OF EIGENVECTORS IN SOLUTION

NORMALIZED DIFFERENCES FGM-VHM

ΔB^{ϕ}

10 %
0
-10 %

ΔB^{θ}

50 %
20 %
0
-20 %
50 %

ΔB^{R}

50 %
20 %
0
-20 %
50 %

6 5 4 3 2 2 3 4 5 6

R (R_J)

***** ITERATION NUMBER   3 **

    GSFC PIONEER 11 AT JUPITER RC 5 RJ
    INTERNAL   3 EXTERNAL 0 ORDER OF FIT
    1500 OBSERVATIONS
    NUMBER OF EIGENVECTORS =   15
    PARAMETER VECTOR :

     4.184 -0.442   0.528 -0.210 -0.888   0.355 -0.061 -0.435 -0.223
    -0.319   0.647 -0.305 -0.537   0.116   0.314

    SINGULAR VALUES OF A

        1   2   3   4   5   6   7   8   9   10   11   12   13   14   15

    1 653.717 430.400 373.533 352.283 224.787 210.074 123.227 103.547 85.552 63.639 58.931 44.022 25.270 16.874 10.837

    V MATRIX

        1   2   3   4   5   6   7   8   9   10   11   12   13   14   15

     1   0.614 -0.364   0.478 -0.057 -0.001 -0.321   0.248 -0.072   0.085 -0.074   0.038 -0.204   0.104 -0.048 -0.140
     2 -0.163 -0.705 -0.175 -0.035 -0.347   0.336   0.167 -0.208 -0.346   0.107   0.034 -0.002   0.043 -0.069 -0.029
     3 -0.524   0.113   0.527 -0.381 -0.321 -0.139 -0.009 -0.198   0.065   0.047 -0.162 -0.220 -0.192   0.036 -0.090
     4 -0.125   0.123 -0.194   0.383 -0.276 -0.566   0.203 -0.052 -0.332 -0.276 -0.300 -0.033   0.152   0.067 -0.022
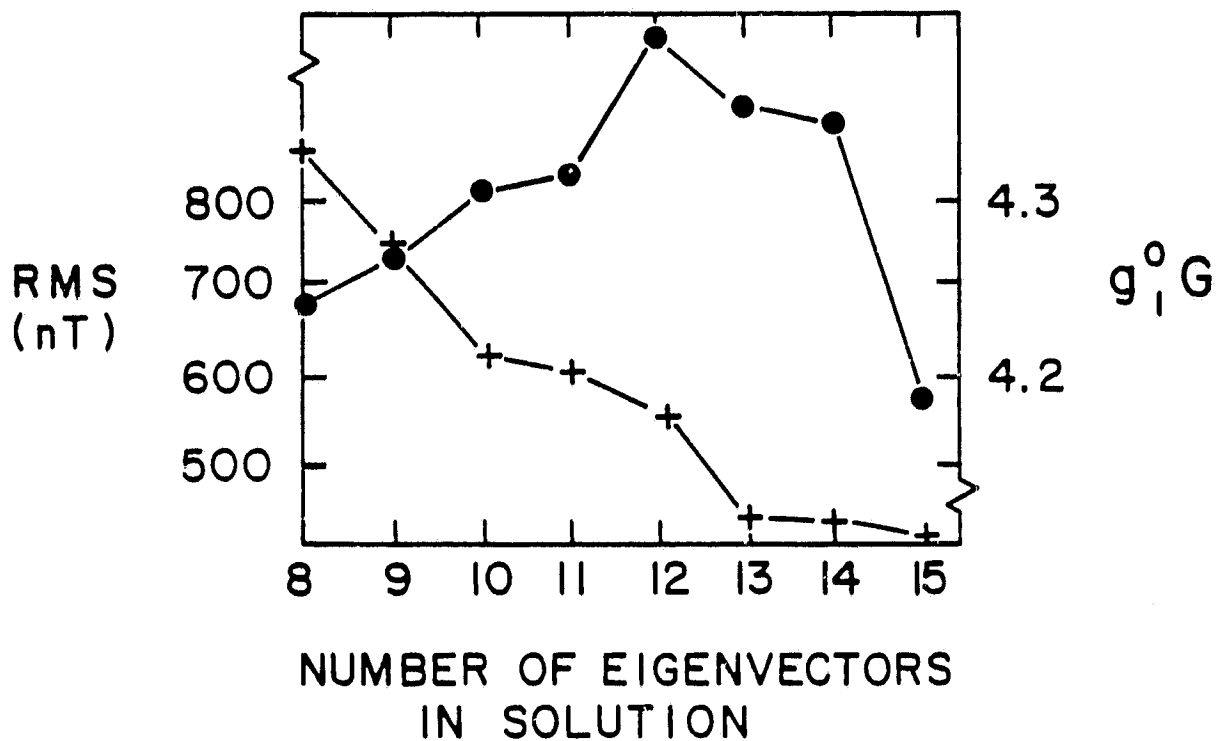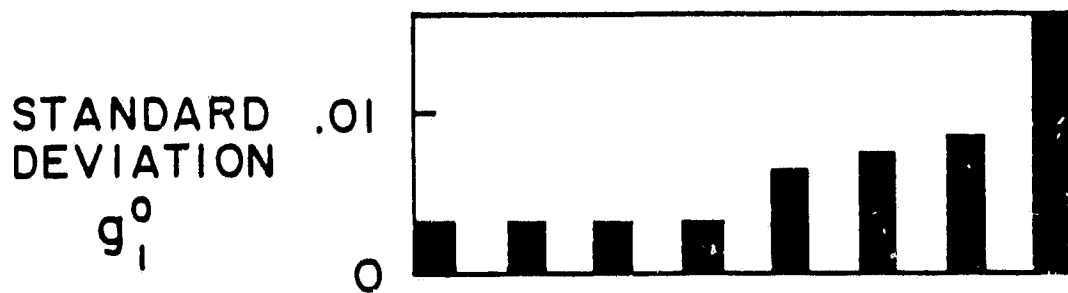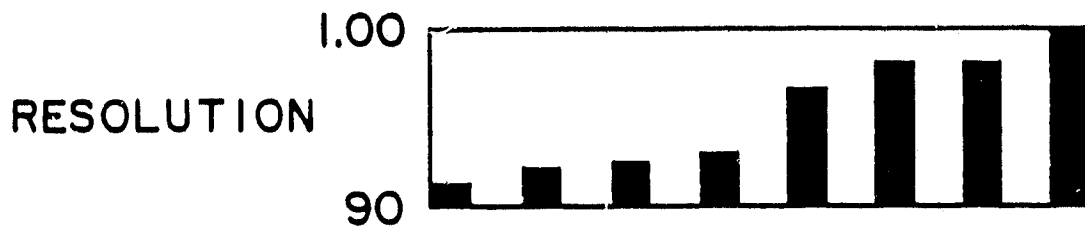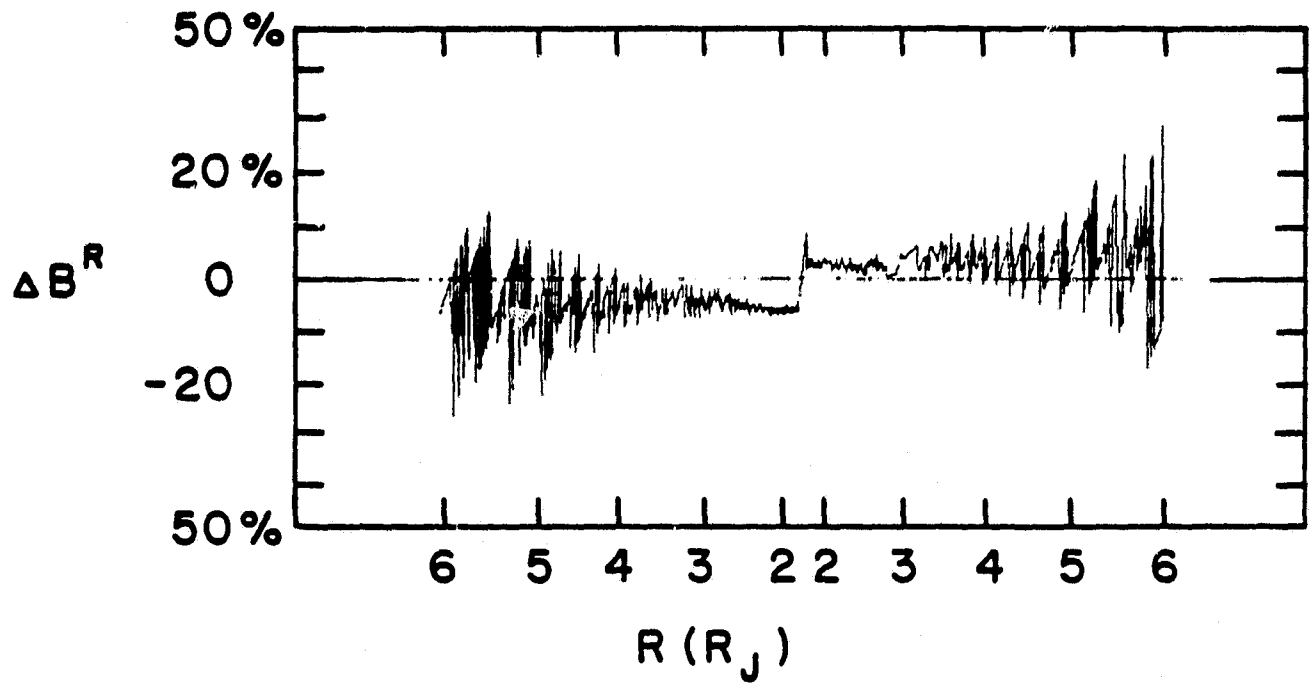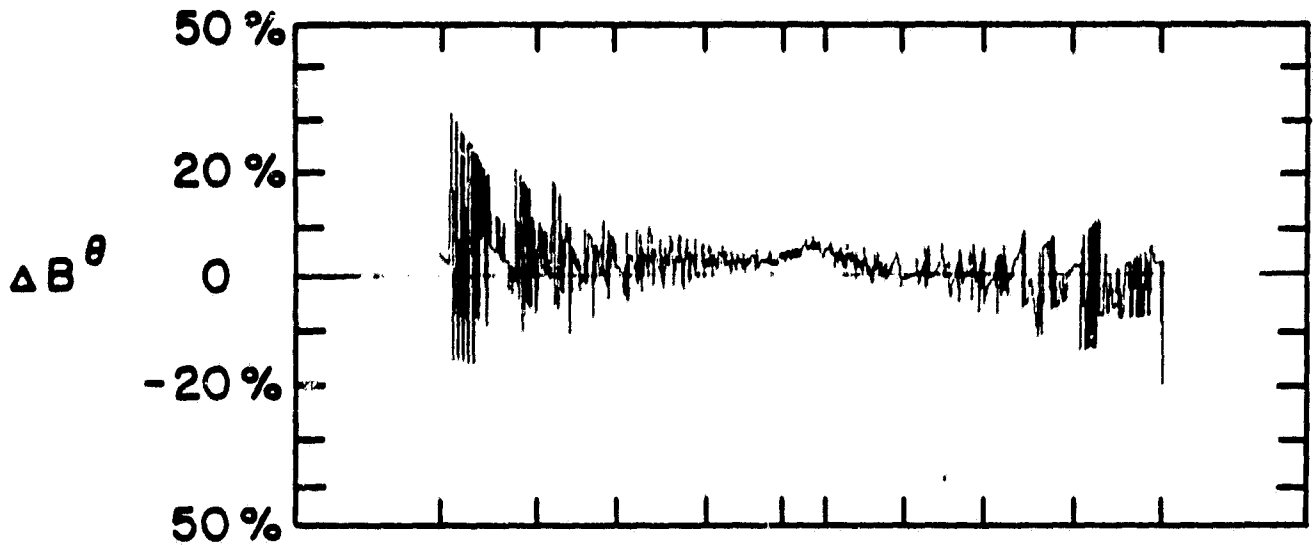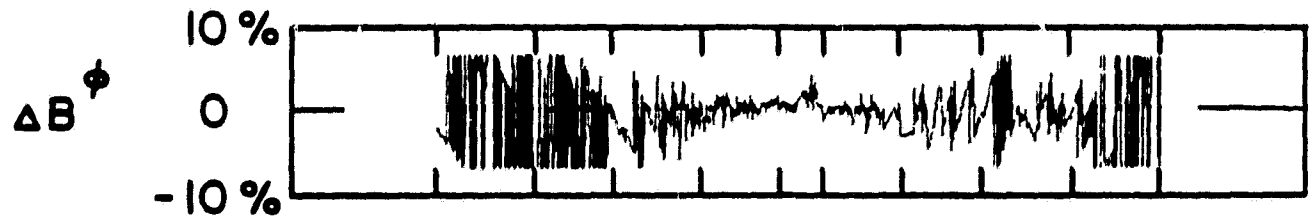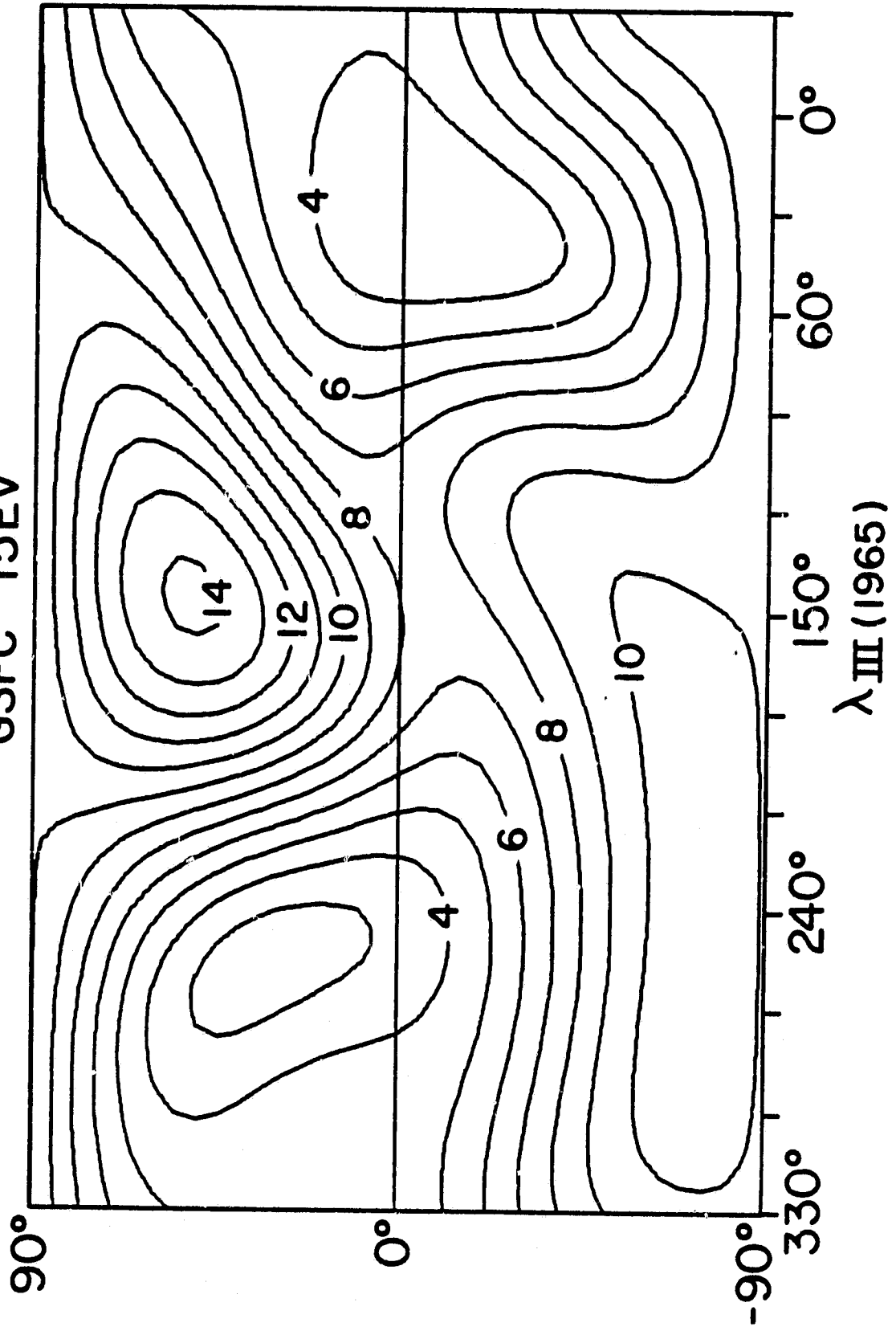   5   0.224   0.191   0.322   0.279 -0.410   0.238 -0.472   0.204 -0.260   0.217 -0.109   0.063   0.192 -0.197 -0.192
     6   0.088 -0.026 -0.297 -0.199 -0.515 -0.291 -0.329 -0.030   0.282 -0.224   0.482   0.013 -0.012 -0.103   0.062
     7   0.311   0.211 -0.317 -0.589 -0.250   0.149   0.224 -0.066   0.015 -0.367 -0.117   0.073   0.102 -0.064
     8 -0.121 -0.193 -0.023 -0.301   0.318 -0.389 -0.190   0.475 -0.406   0.134   0.183   0.023   0.008 -0.130 -0.231
     9 -0.099 -0.039   0.115 -0.290   0.134   0.010 -0.116 -0.240   0.050 -0.283 -0.143   0.529   0.642 -0.050 -0.066
    10 -0.079 -0.126 -0.091   0.115 -0.076 -0.217   0.183   0.115   0.444   0.456 -0.359   0.288 -0.035 -0.479   0.044
    11 -0.147   0.105   0.251   0.009 -0.137   0.087   0.381   0.397 -0.065   0.010   0.305 -0.040   0.352 -0.073   0.589
    12   0.070   0.151 -0.073 -0.038 -0.101 -0.210   0.085 -0.260 -0.034   0.664   0.274   0.143   0.229   0.490 -0.072
    13 -0.227   0.111 -0.133   0.158   0.028   0.147   0.233   0.065   0.269 -0.021   0.201 -0.403   0.398 -0.170 -0.591
    14   0.154   0.331 -0.037 -0.148   0.110   0.034   0.224 -0.458 -0.359   0.088   0.185   0.006 -0.110 -0.595   0.026
    15   0.004 -0.095 -0.148 -0.052   0.186 -0.086 -0.383 -0.215   0.014   0.190 -0.248 -0.536   0.353 -0.099   0.394

FARAMETERS AND PARAMETER ADJUSTMENTS, ITERATION #   3

WEIGHTED RMS DEVIATION 0.00504 EXTERNAL
WEIGHTED RMS DEVIATION 0.00500 INTERNAL

J = 1 PARAMETER =   4.184 ADJ =   0.000 STD DEV = 0.0150 (0.00211) LIN = 0.7997
         0.015   0.003   0.006   0.003   0.018 -0.004   0.007   0.020   0.009 -0.002 -0.041   0.001   0.056   0.004 -0.023
J = 2 PARAMETER = -0.442 ADJ =   0.000 STD DEV = 0.0077 (0.00288) LIN = 0.7948
         0.006   0.008   0.000   0.001. 0.015   0.001   0.000   0.014   0.008   0.011 -0.013 -0.008   0.026   0.021 -0.006
J = 3 PARAMETER =   0.528 ADJ =   0.000 STD DEV = 0.0132 (0.00233) LIN = 0.7565
         0.007   0.000   0.013   0.000   0.005 -0.008   0.006   0.010 -0.015 -0.008 -0.044   0.002   0.026 -0.005 -0.025
J = 4 PARAMETER = -0.210 ADJ =   0.000 STD DEV = 0.0116 (0.00432) LIN = 0.6273
         0.004   0.001 -0.001   0.012   0.003 -0.009   0.008 -0.001   0.015 -0.013 -0.006   0.010   0.012 -0.015   0.000
J = 5 PARAMETER = -0.888 ADJ =   0.000 STD DEV = 0.0236 (0.00383) LIN = 0.5660
         0.011   0.005   0.003   0.001   0.024 -0.001   0.004   0.022   0.014   0.010 -0.034 -0.005   0.049   0.014 -0.020
J = 6 PARAMETER =   0.355 ADJ =   0.000 STD DEV = 0.0170 (0.00493) LIN = 0.6022
        -0.004   0.001 -0.006 -0.006 -0.002   0.017 -0.011 -0.002 -0.001   0.018   0.028 -0.022 -0.016   0.025   0.017
J = 7 PARAMETER = -0.061 ADJ =   0.000 STD DEV = 0.0131 (0.00297) LIN = 0.6908
         0.008   0.000   0.006   0.007   0.007 -0.014   0.013   0.007   0.006 -0.015 -0.032   0.016   0.031 -0.021 -0.017
J = 8 PARAMETER = -0.435 ADJ =   0.000 STD DEV = 0.0252 (0.00445) LIN = 0.5027
         0.012   0.004   0.005   0.000   0.021 -0.002   0.004   0.025   0.006   0.006 -0.042 -0.005   0.053   0.013 -0.023
J = 9 PARAMETER = -0.223 ADJ =   0.000 STD DEV = 0.0295 (0.00713) LIN = 0.3346
         0.005   0.002 -0.007   0.006   0.011 -0.001   0.003   0.005   0.029   0.002   0.000   0.006   0.022 -0.001   0.000
J = 10 PARAMETER = -0.319 ADJ =   0.000 STD DEV = 0.0317 (0.00814) LIN = 0.3140
        -0.001   0.003 -0.003 -0.005   0.008   0.010 -0.006   0.005   0.002   0.032   0.012 -0.026 -0.004   0.031   0.010
J = 11 PARAMETER =   0.647 ADJ =   0.000 STD DEV = 0.0565 (0.00623) LIN = 0.3411
        -0.011 -0.002 -0.010 -0.001 -0.014   0.008 -0.007 -0.019   0.000   0.007   0.057 -0.006 -0.047   0.004   0.038
J = 12 PARAMETER = -0.305 ADJ =   0.000 STD DEV = 0.0335 (0.00883) LIN = 0.2904
         0.001 -0.002   0.001   0.004 -0.004 -0.011   0.006 -0.004   0.005 -0.024 -0.010   0.033   0.006 -0.031 -0.009
J = 13 PARAMETER = -0.537 ADJ =   0.000 STD DEV = 0.0584 (0.00551) LIN = 0.3183
         0.014   0.003   0.006   0.002   0.020 -0.005   0.007   0.022   0.011 -0.002 -0.045   0.003   0.058   0.003 -0.027
J = 14 PARAMETER =   0.116 ADJ =   0.000 STD DEV = 0.0363 (0.00478) LIN = 0.4535
         0.001   0.004 -0.002 -0.005   0.009   0.011 -0.007   0.009 -0.001   0.027   0.006 -0.028   0.004   0.036   0.006
J = 15 PARAMETER =   0.314 ADJ =   0.000 STD DEV = 0.0419 (0.00954) LIN = 0.3618
        -0.008 -0.001 -0.008   0.000 -0.011   0.007 -0.005 -0.017   0.000   0.008   0.051 -0.007 -0.033   0.005   0.042

JOVIAN SURFACE ISOINTENSITY CONTOUR MAP
GSFC 15EV

JOVIAN SURFACE ISOINTENSITY CONTOUR MAPS
P11 GSFC FLUXGATE DATA
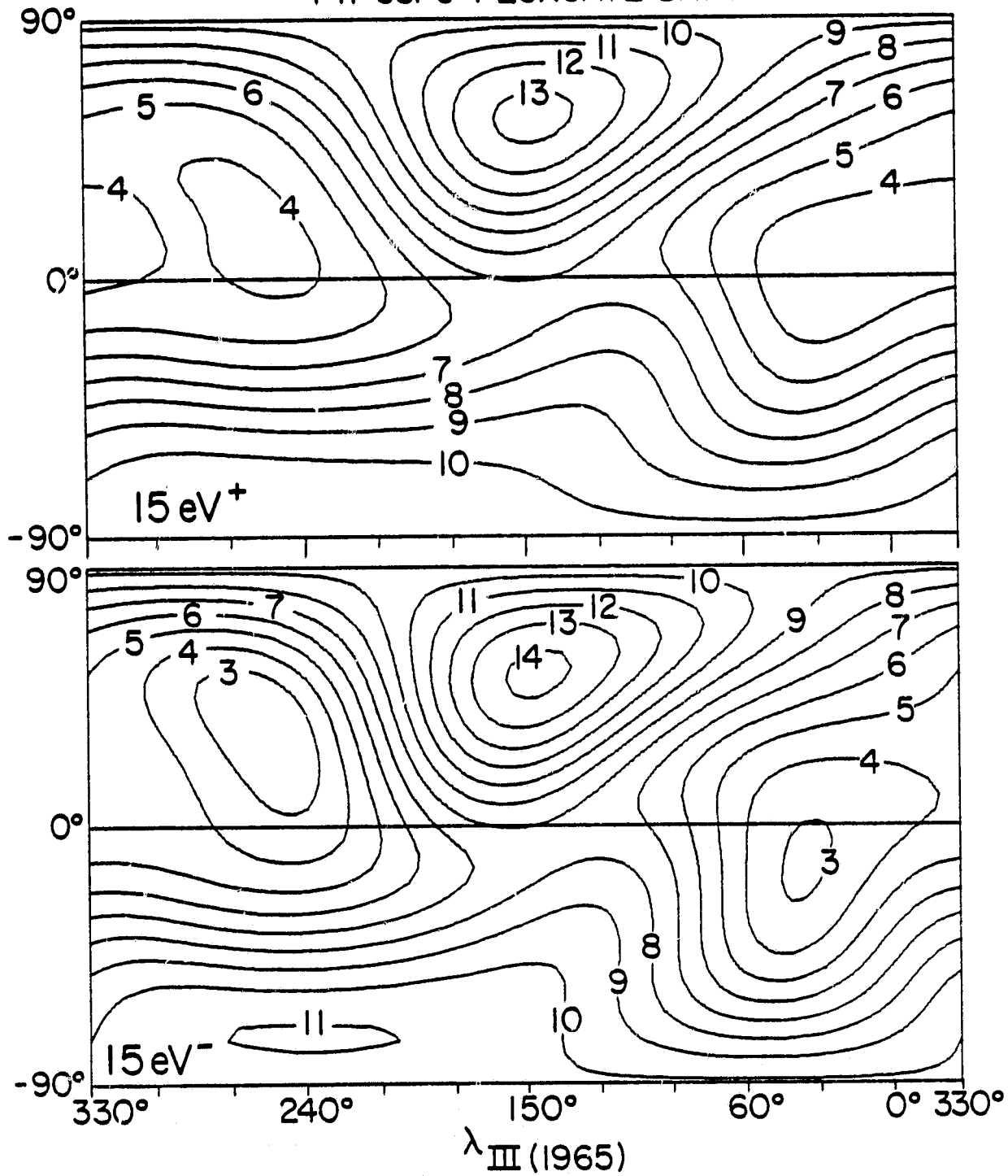
15 eV⁺

15 eV⁻

λ_{III} (1965)

***** ITERATION NUMBER   3 ***

    GSFC PIONEER 11 AT JUPITER R < 5 RJ
    INTERNAL   3 EXTERNAL   0 ORDER OF FIT
    1550 OBSERVATIONS
    NUMBER OF EIGENVECTORS =   13
    PARAMETER VECTOR :

        4.352 -0.396   0.624 -0.197 -0.635   0.295   0.015 -0.139 -0.138
       -0.307 -0.015 -0.312   0.117   0.194 -0.122

        SINGULAR VALUES OF A

         1   2   3   4   5   6   7   8   9   10   11   12   13   14   15

    1 656.201 431.931 373.082 353.699 226.516 208.427 122.960 103.226 85.675 62.979 59.562 43.692 25.229 16.934 10.855

        V MATRIX

         1   2   3   4   5   6   7   8   9   10   11   12   13   14   15

     1   0.615 -0.363   0.471 -0.075 -0.025 -0.331   0.243 -0.071   0.086 -0.069   0.056 -0.201   0.105   0.049 -0.139
     2 -0.159 -0.708 -0.177 -0.038   0.363   0.309   0.167 -0.220 -0.344   0.107   0.019 -0.001   0.043   0.069 -0.029
     3 -0.525   0.113   0.523 -0.384   0.314 -0.160 -0.012 -0.201   0.065   0.010 -0.161 -0.227 -0.189 -0.037 -0.090
     4 -0.126   0.120 -0.193   0.384   0.232 -0.588   0.202 -0.057 -0.336 -0.327 -0.236 -0.034   0.152 -0.070 -0.023
     5   0.225   0.130   0.330   0.283   0.418   0.212 -0.465   0.200 -0.266   0.196 -0.162   0.053   0.194   0.199 -0.190
     6   0.088 -0.023 -0.299 -0.190   0.504 -0.319 -0.336 -0.007   0.236 -0.124   0.506   0.029 -0.015   0.192   0.082
     7   0.309   0.225 -0.323 -0.578   0.267   0.145   0.234   0.276 -0.072 -0.063 -0.379 -0.127   0.075 -0.103 -0.083
     8 -0.192 -0.189 -0.036 -0.312 -0.338 -0.358 -0.133   0.480 -0.407   0.228   0.136   0.016   0.009   0.182 -0.230
     9 -0.100 -0.033   0.111 -0.273 -0.132   0.017 -0.122 -0.234   0.050 -0.200 -0.092   0.539   0.637   0.046 -0.068
    10 -0.079 -0.136 -0.094   0.110   0.077 -0.221   0.187   0.103   0.438   0.378 -0.461   0.269 -0.036   0.479   0.062
    11 -0.146   0.100   0.254   0.011   0.144   0.077   0.337   0.392 -0.066   0.066   0.292 -0.029   0.349   0.031   0.572
    12   0.069   0.153 -0.078 -0.035   0.090 -0.214   0.032 -0.262 -0.025   0.708   0.143   0.132   0.233 -0.486 -0.067
    13 -0.226   0.106 -0.127   0.166 -0.016   0.149   0.234   0.064   0.272   0.008   0.212 -0.395   0.401   0.173 -0.583
    14   0.142   0.336 -0.035 -0.141 -0.105   0.039   0.217 -0.464 -0.351   0.115   0.131   0.016 -0.115   0.593   0.021
    15   0.003 -0.089 -0.154 -0.052 -0.195 -0.067 -0.332 -0.221   0.014   0.121 -0.260 -0.591   0.356   0.105   0.398

        RESOLUTION MATRIX (V VT)

   1   2   3   4   5   6   7   8   9   10   11   12   13   14   15

     1   0.978 -0.007 -0.011   0.000 -0.036   0.002 -0.006 -0.041 -0.012 -0.015   0.078   0.015 -0.090 -0.026   0.050
     2 -0.007   0.994   0.000   0.004 -0.019 -0.011   0.005 -0.019 -0.005 -0.031   0.012   0.031 -0.029 -0.040   0.004
     3 -0.011   0.000   0.991 -0.005 -0.010   0.014 -0.011 -0.014 -0.004   0.023   0.056 -0.024 -0.046   0.024   0.040
     4   0.000   0.004 -0.005   0.995   0.010   0.015 -0.009   0.007   0.002   0.035   0.019 -0.035 -0.001   0.042   0.016
     5 -0.036 -0.019 -0.010   0.010   0.924 -0.023   0.005 -0.080 -0.022 -0.084   0.097   0.084 -0.146 -0.114   0.055
     6   0.002 -0.011   0.014   0.015 -0.023   0.957   0.027 -0.016 -0.003 -0.097 -0.064   0.029   0.015 -0.115 -0.053
     7 -0.006   0.005 -0.011 -0.009   0.005   0.027   0.983   0.000 -0.001   0.055   0.057 -0.056 -0.031   0.063   0.044
     8 -0.041 -0.019 -0.014   0.007 -0.080 -0.016   0.000   0.914 -0.024 -0.073   0.122   0.073 -0.167 -0.103   0.073
     9 -0.012 -0.005 -0.004   0.002 -0.022 -0.003 -0.001 -0.024   0.993 -0.018   0.037   0.018 -0.048 -0.026   0.022
    10 -0.015 -0.031   0.023   0.035 -0.084 -0.097   0.055 -0.073 -0.018   0.767 -0.076   0.237 -0.046 -0.285 -0.075
    11   0.078   0.012   0.056   0.019   0.097 -0.064   0.057   0.122   0.037 -0.076   0.643   0.079   0.334 -0.060 -0.244
    12   0.015   0.031 -0.024 -0.035   0.084   0.099 -0.056   0.073   0.018   0.237   0.079   0.759   0.045   0.289   0.078
    13 -0.090 -0.029 -0.046 -0.001 -0.146   0.015 -0.031 -0.167 -0.048 -0.046   0.334   0.045   0.624 -0.090   0.216
    14 -0.026 -0.040   0.024   0.042 -0.114 -0.115   0.063 -0.103 -0.026 -0.285 -0.060   0.289 -0.090   0.648 -0.071
    15   0.050   0.004   0.040   0.016   0.055 -0.053   0.044   0.073   0.022 -0.075 -0.244   0.078   0.216 -0.071   0.831

PARAMETERS AND PARAMETER ADJUSTMENTS, ITERATION #   3

WEIGHTED RMS DEVIATION 0.00530 EXTERNAL
WEIGHTED RMS DEVIATION 0.00500 INTERNAL

    J = 1   PARAMETER =   4.352 ADJ =   0.000 STD DEV = 0.0072 (0.00211) LIN = 0.7987
    J = 2   PARAMETER = -0.396 ADJ =   0.000 STD DEV = 0.0060 (0.00287) LIN = 0.7968
    J = 3   PARAMETER =   0.624 ADJ =   0.000 STD DEV = 0.0101 (0.00233) LIN = 0.7559
    J = 4   PARAMETER = -0.197 ADJ =   0.000 STD DEV = 0.0107 (0.00433) LIN = 0.6245
    J = 5   PARAMETER = -0.635 ADJ =   0.000 STD DEV = 0.0105 (0.00382) LIN = 0.5587
    J = 6   PARAMETER =   0.295 ADJ =   0.000 STD DEV = 0.0102 (0.00493) LIN = 0.6032
    J = 7   PARAMETER =   0.015 ADJ =   0.000 STD DEV = 0.0067 (0.00297) LIN = 0.6921
    J = 8   PARAMETER = -0.139 ADJ =   0.000 STD DEV = 0.0084 (0.00444) LIN = 0.5025
    J = 9   PARAMETER = -0.138 ADJ =   0.000 STD DEV = 0.0287 (0.00709) LIN = 0.3350
    J = 10   PARAMETER = -0.307 ADJ =   0.000 STD DEV = 0.0129 (0.00319) LIN = 0.3106
    J = 11   PARAMETER = -0.015 ADJ =   0.000 STD DEV = 0.0156 (0.00622) LIN = 0.3421
    J = 12   PARAMETER = -0.312 ADJ =   0.000 STD DEV = 0.0153 (0.00382) LIN = 0.2904
    J = 13   PARAMETER =   0.117 ADJ =   0.000 STD DEV = 0.0191 (0.00552) LIN = 0.3176
    J = 14   PARAMETER =   0.194 ADJ =   0.000 STD DEV = 0.0086 (0.00477) LIN = 0.4552
    J = 15   PARAMETER = -0.122 ADJ =   0.000 STD DEV = 0.0205 (0.00948) LIN = 0.3636
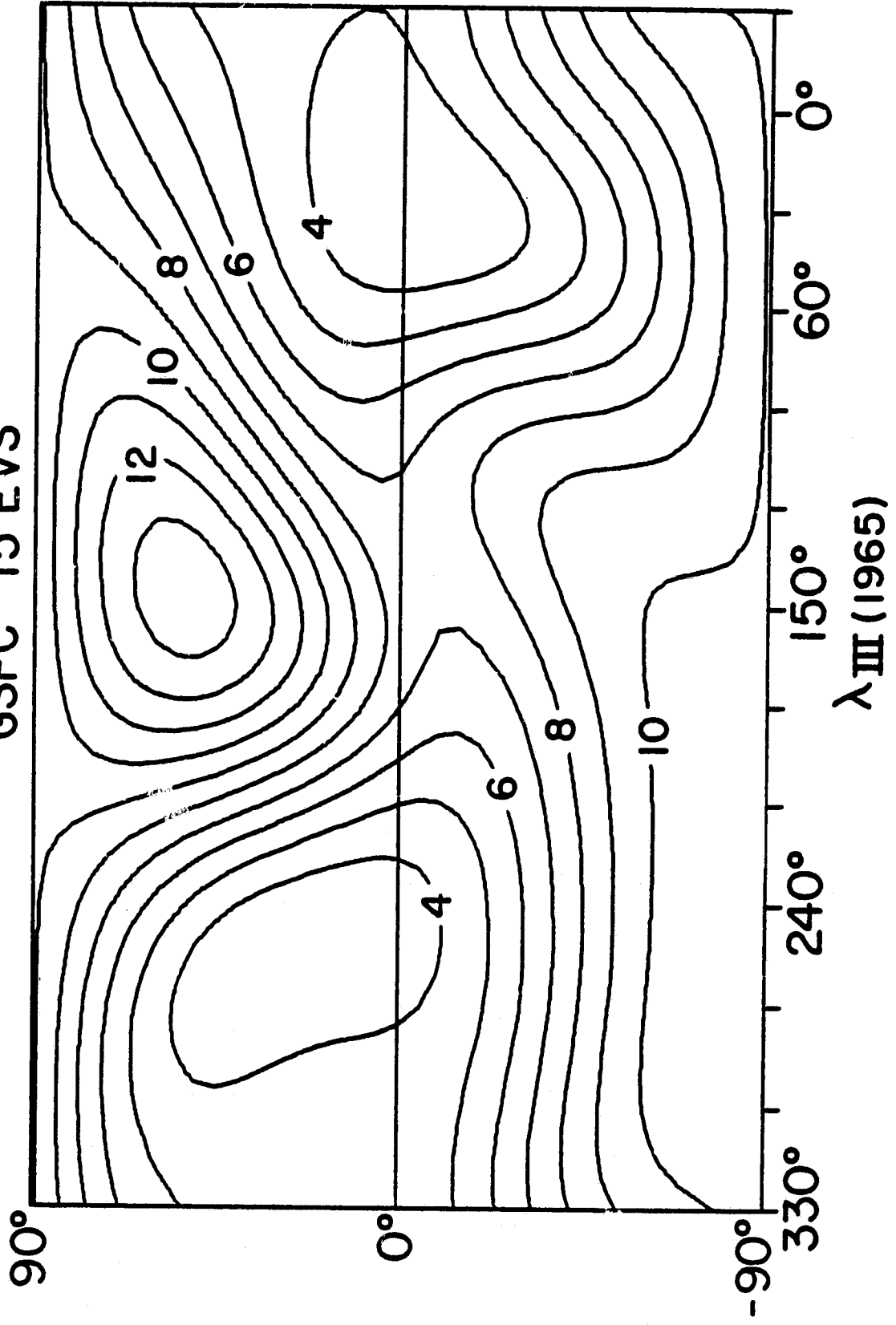
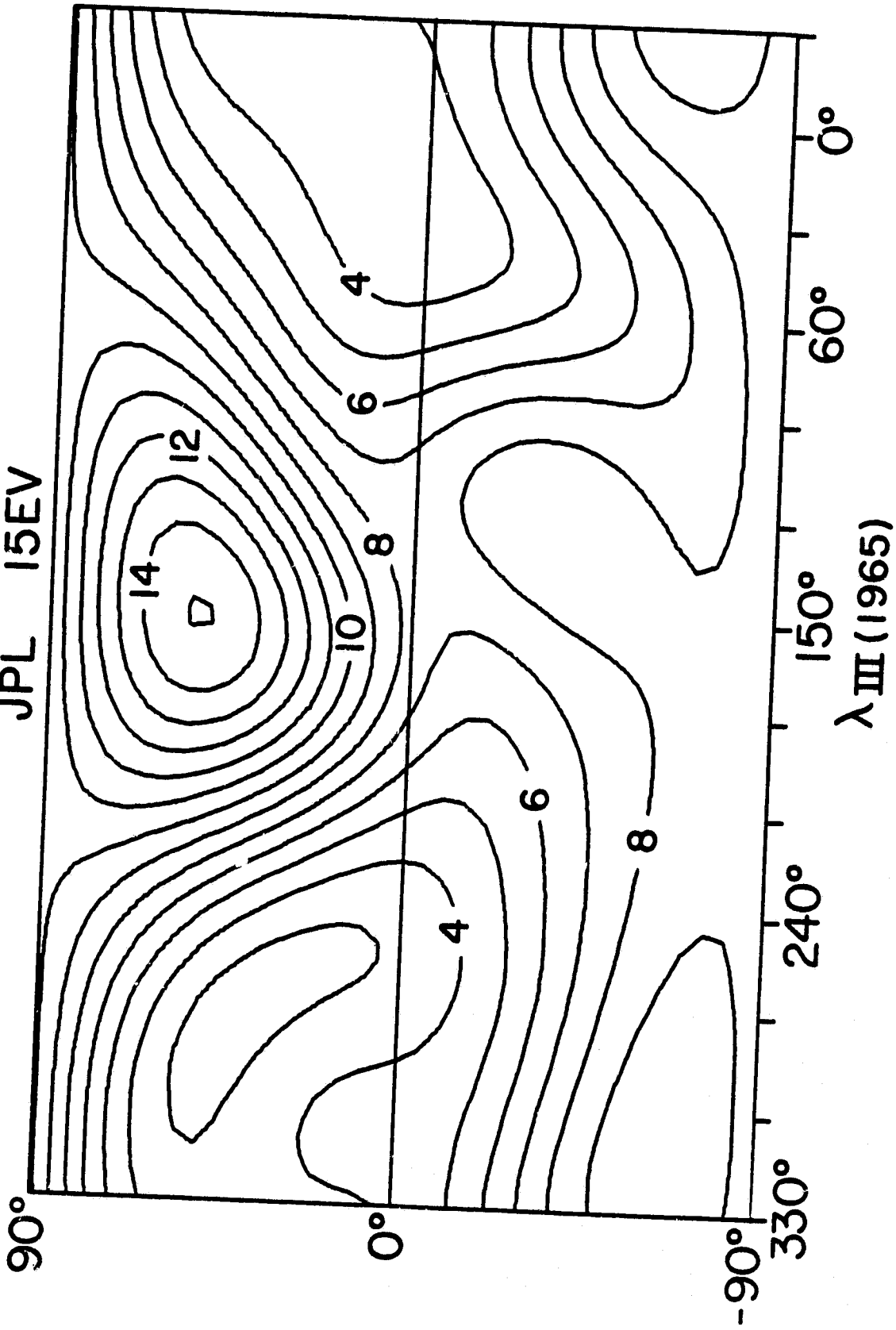JOVIAN SURFACE ISOINTENSITY CONTOUR MAP
GSFC 13EV
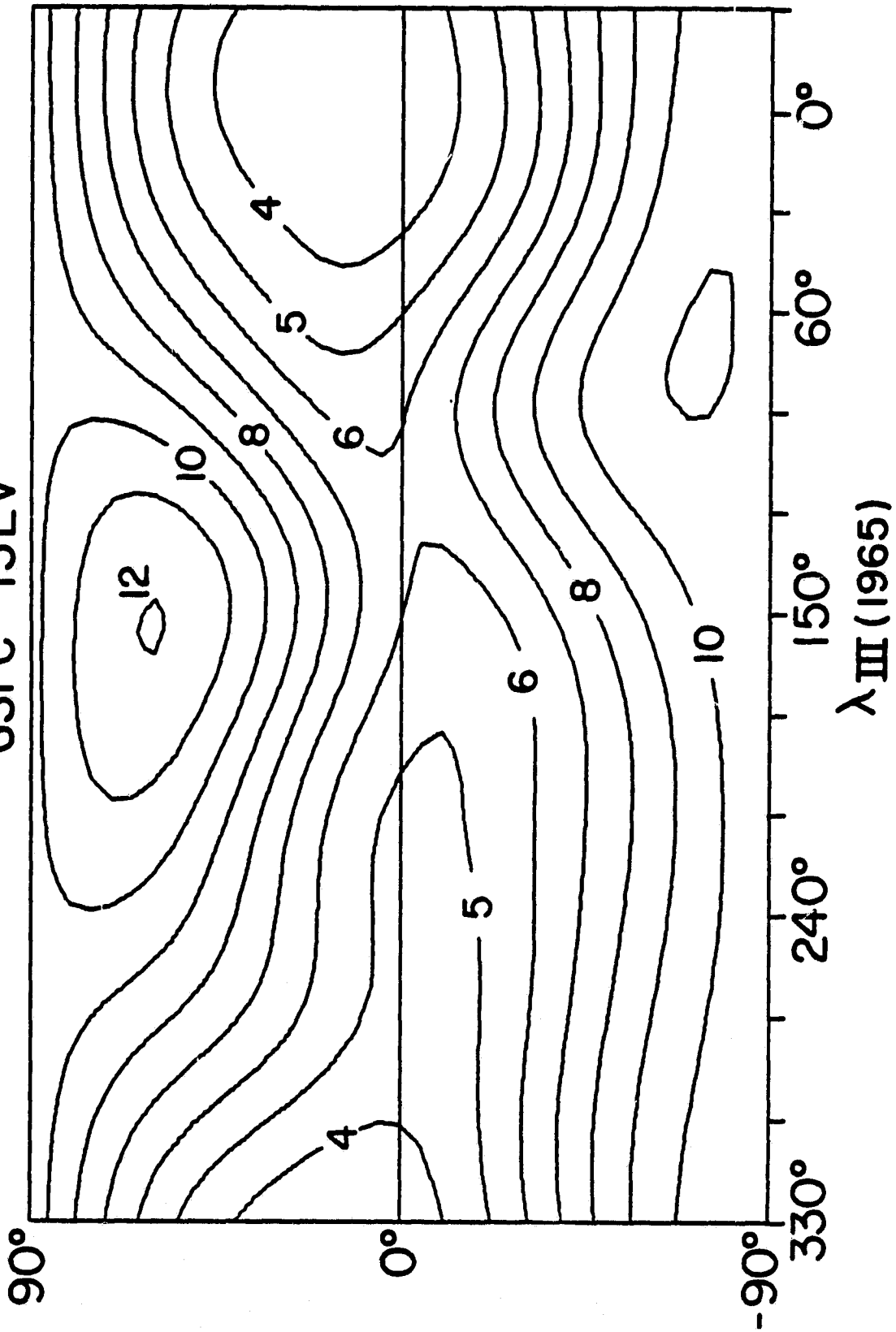
JOVIAN SURFACE ISOINTENSITY CONTOUR MAP
GSFC 15 EVS

JOVIAN SURFACE ISOINTENSITY CONTOUR MAP
JPL I5EV

++++ ITERATION NUMBER 2 ++

JPL PIONEER 11 AT JUPITER R < 5 RJ
INTERNAL   3 EXTERNAL 0 ORDER OF FIT
972 OBSERVATIONS
NUMBER OF EIGENVECTORS =   15
PARAMETER VECTOR :

    4.064 -0.452   0.567 -0.098 -0.934   0.368 -0.101 -0.423 -0.306
   -0.596   0.528 -0.261 -0.365   0.014   0.351

    SINGULAR VALUES OF A

      1   2   3   4   5   6   7   8   9   10   11   12   13   14   15

   1 487.543 388.907 370.964 249.973 230.272 176.354 136.281 124.348 104.962 91.721 71.262 45.689 43.120 32.646 28.903

    V MATRIX

      1   2   3   4   5   6   7   8   9   10   11   12   13   14   15

   1   0.772 -0.235 0.544 0.008 0.128 -0.013 0.018 -0.022 0.012 -0.081 0.032 -0.042 -0.159 0.027 0.019
   2   0.257 0.896 0.049 0.152 -0.186 -0.162 0.075 -0.080 -0.124 0.067 -0.067 -0.033 -0.064 0.042 -0.030
   3 -0.514 0.170 0.775 -0.140 0.133 0.096 0.146 -0.009 0.065 0.043 0.009 -0.143 0.047 0.010 0.081
   4 -0.089 -0.081 0.067 -0.282 -0.174 -0.745 -0.201 -0.396 0.220 -0.220 -0.104 0.032 -0.048 0.019 0.037
   5 -0.041 0.055 -0.204 -0.197 0.589 -0.286 0.529 0.133 -0.170 -0.178 0.037 -0.069 -0.325 0.124 -0.015
   6 -0.083 -0.028 0.101 0.327 0.332 -0.394 -0.425 0.351 -0.026 0.493 -0.023 0.078 -0.078 0.101 -0.199
   7 -0.117 -0.064 0.004 0.822 0.120 -0.052 0.164 -0.271 0.284 -0.304 0.062 -0.064 -0.049 -0.003 0.079
   8 -0.101 -0.205 0.081 0.157 -0.589 -0.209 0.179 0.449 -0.237 -0.099 -0.072 -0.328 -0.252 0.209 0.061
   9 -0.073 -0.039 0.112 0.086 -0.080 0.085 0.153 0.087 -0.064 -0.040 -0.572 0.694 -0.231 -0.183 0.021
  10   0.015 0.037 0.058 -0.013 -0.162 -0.084 0.199 0.204 0.190 0.011 0.607 0.578 0.133 0.237 0.103
  11 -0.084 0.073 0.114 0.016 0.028 0.059 -0.264 0.137 -0.257 -0.612 0.136 0.105 0.057 -0.009 -0.639
  12 -0.055 -0.072 0.074 0.101 -0.044 -0.189 0.041 -0.118 -0.521 0.088 0.405 0.089 -0.018 -0.660 0.188
  13 -0.107 0.104 -0.050 -0.083 -0.011 0.253 -0.391 -0.085 0.109 -0.057 0.275 -0.002 -0.787 0.045 0.178
  14 -0.079 -0.153 0.048 0.082 -0.021 0.089 0.032 -0.547 -0.538 0.213 -0.016 0.096 -0.037 0.544 -0.105
  15 -0.009 -0.090 -0.001 -0.037 -0.217 0.003 0.353 -0.173 0.288 0.361 0.140 -0.062 -0.258 -0.212 -0.664


PARAMETERS AND PARAMETER ADJUSTMENTS, ITERATION #   2

WEIGHTED RMS DEVIATION 0.00093 EXTERNAL
WEIGHTED RMS DEVIATION 0.00126 INTERNAL

J = 1 PARAMETER =   4.064 ADJ =   0.000 STD DEV = 0.0047 (0.00228) LIN = 0.9515
J = 2 PARAMETER = -0.452 ADJ =   0.000 STD DEV = 0.0040 (0.00265) LIN = 0.9499
J = 3 PARAMETER =   0.567 ADJ =   0.000 STD DEV = 0.0053 (0.00256) LIN = 0.9231
J = 4 PARAMETER = -0.098 ADJ =   0.000 STD DEV = 0.0071 (0.00563) LIN = 0.7710
J = 5 PARAMETER = -0.934 ADJ =   0.000 STD DEV = 0.0103 (0.00525) LIN = 0.7612
J = 6 PARAMETER =   0.368 ADJ =   0.000 STD DEV = 0.0109 (0.00599) LIN = 0.7009
J = 7 PARAMETER = -0.101 ADJ =   0.000 STD DEV = 0.0069 (0.00446) LIN = 0.8384
J = 8 PARAMETER = -0.423 ADJ =   0.000 STD DEV = 0.0128 (0.00528) LIN = 0.6721
J = 9 PARAMETER = -0.306 ADJ =   0.000 STD DEV = 0.0193 (0.01139) LIN = 0.3029
J = 10 PARAMETER = -0.596 ADJ =   0.000 STD DEV = 0.0192 (0.01208) LIN = 0.4544
J = 11 PARAMETER =   0.528 ADJ =   0.000 STD DEV = 0.0236 (0.00982) LIN = 0.3583
J = 12 PARAMETER = -0.261 ADJ =   0.000 STD DEV = 0.0227 (0.01068) LIN = 0.3856
J = 13 PARAMETER = -0.365 ADJ =   0.000 STD DEV = 0.0200 (0.00920) LIN = 0.3571
J = 14 PARAMETER =   0.014 ADJ =   0.000 STD DEV = 0.0186 (0.00826) LIN = 0.4452
J = 15 PARAMETER =   0.351 ADJ =   0.000 STD DEV = 0.0254 (0.01038) LIN = 0.4638

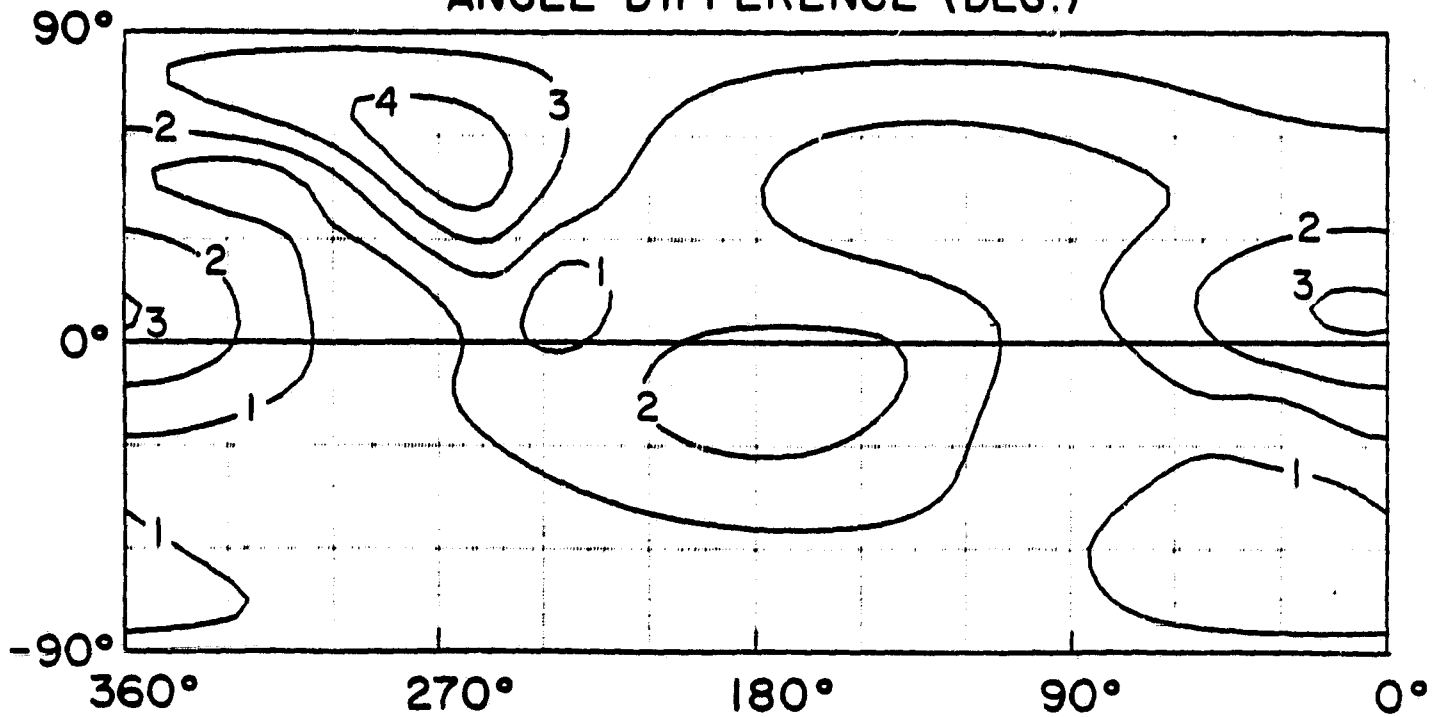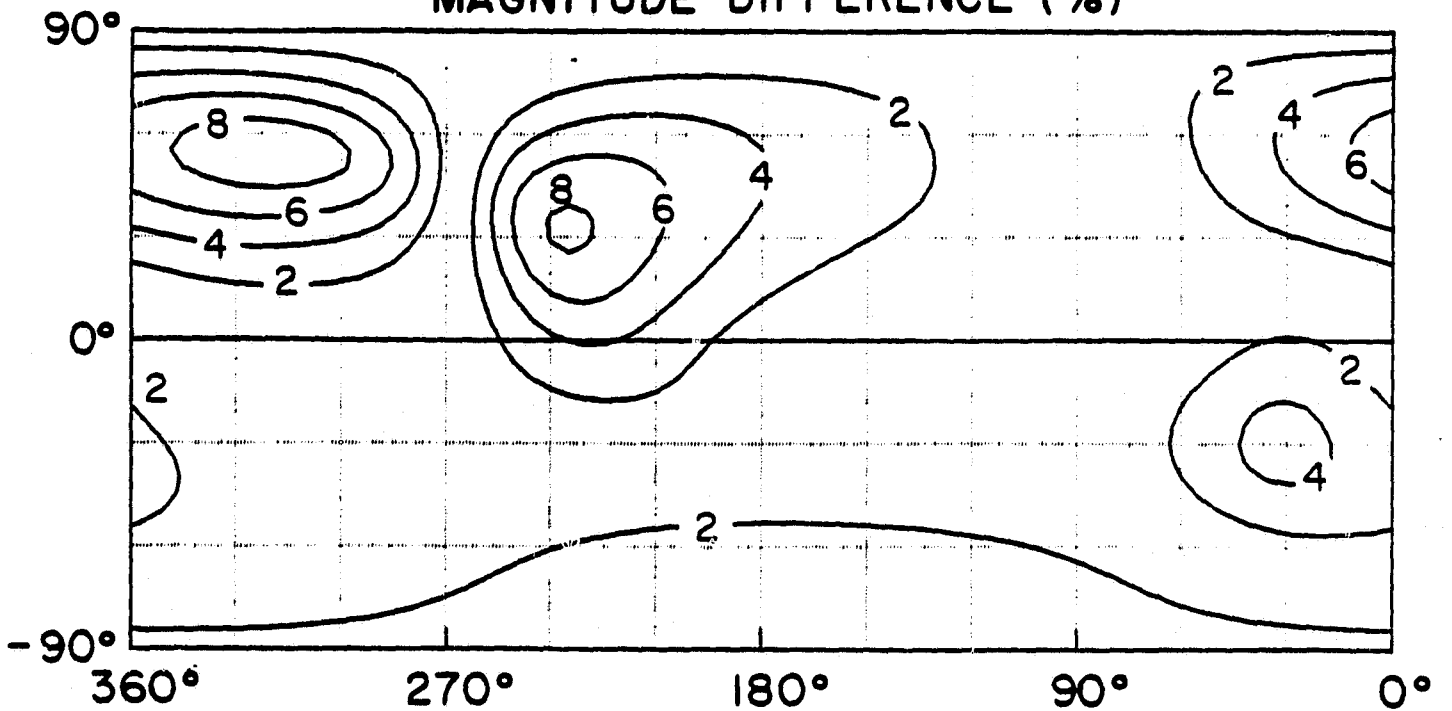JOVIAN SURFACE ISOINTENSITY CONTOUR MAP
JPL 15EVS
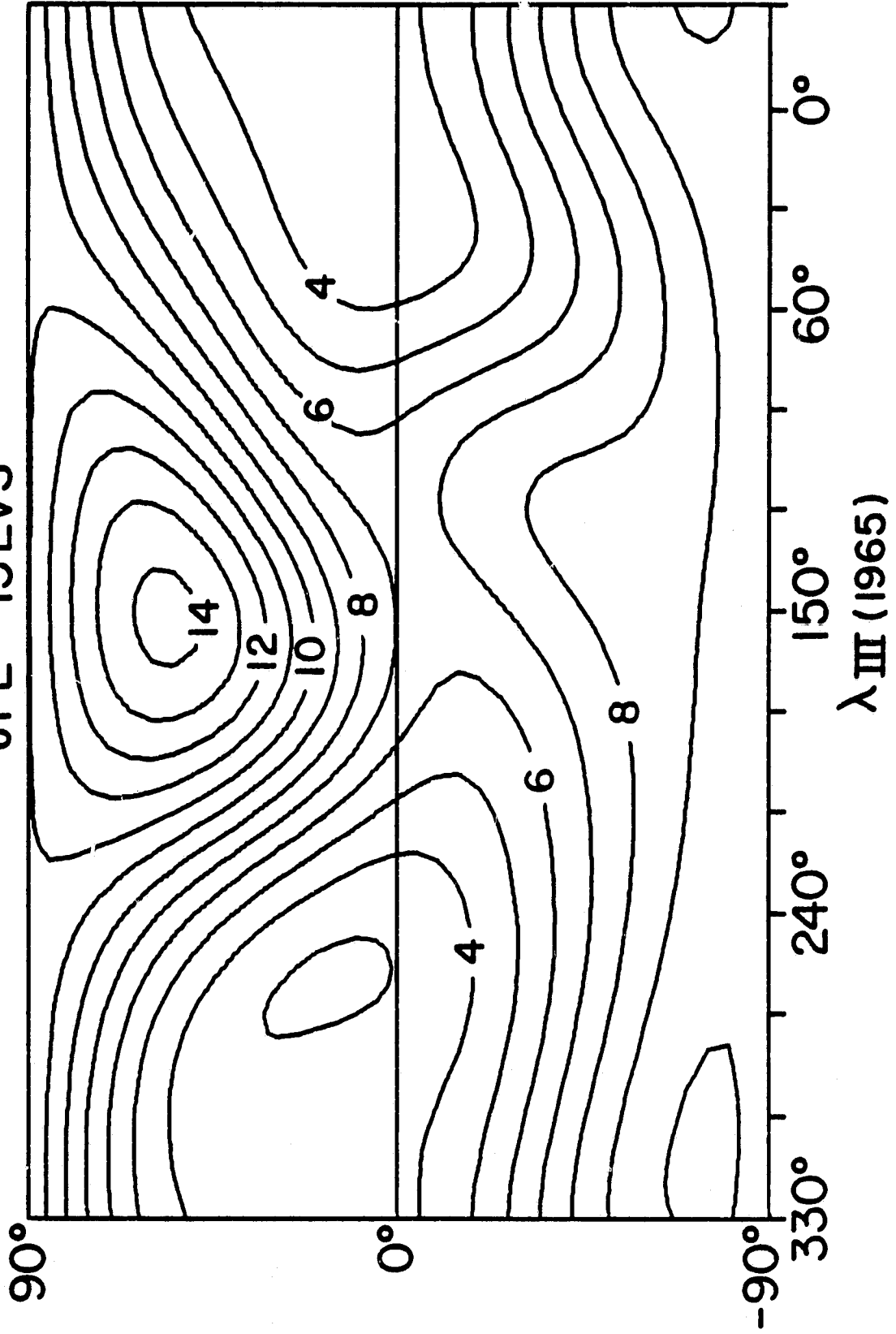
JOVIAN SURFACE CONTOUR MAPS
MODEL DIFFERENCES   GSFC 15 EVS , 04

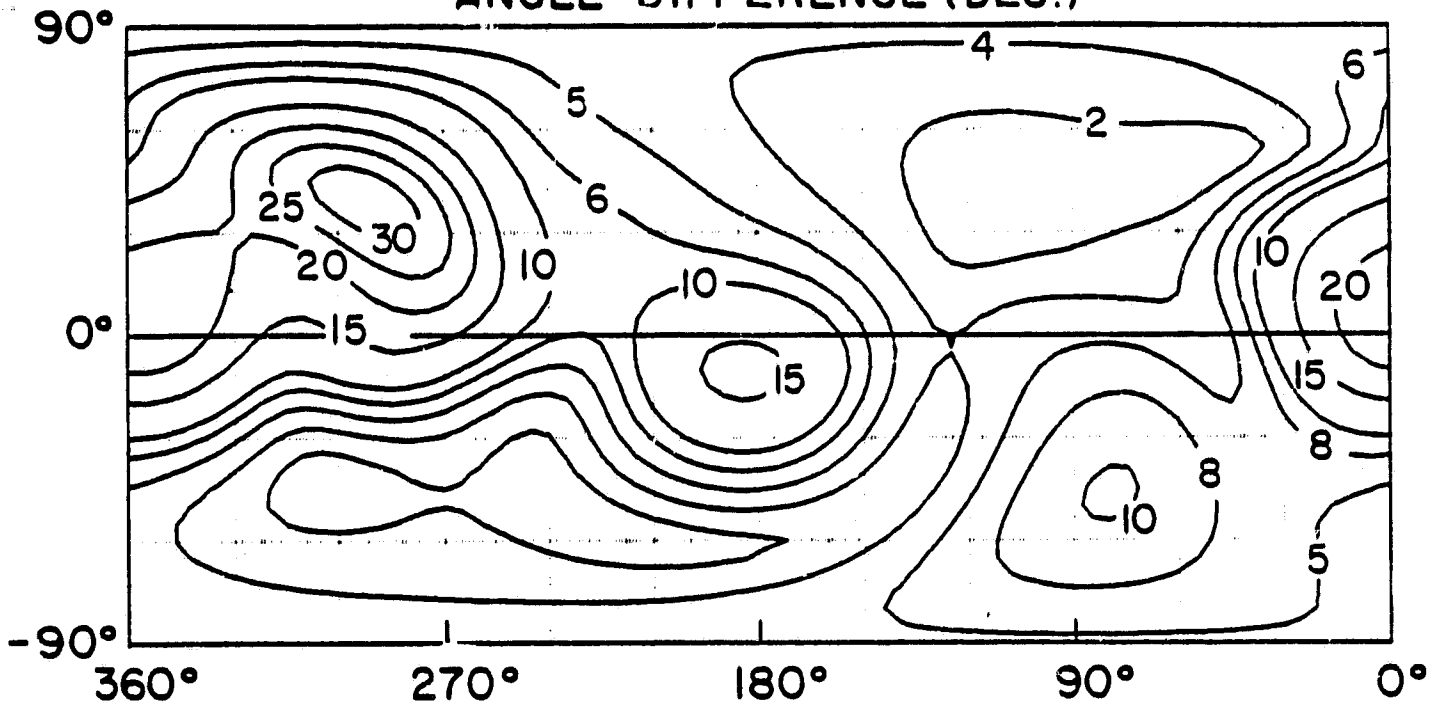
ANGLE DIFFERENCE (DEG.)

MAGNITUDE DIFFERENCE (%)

λ_{III} (1965)

JOVIAN SURFACE CONTOUR MAPS
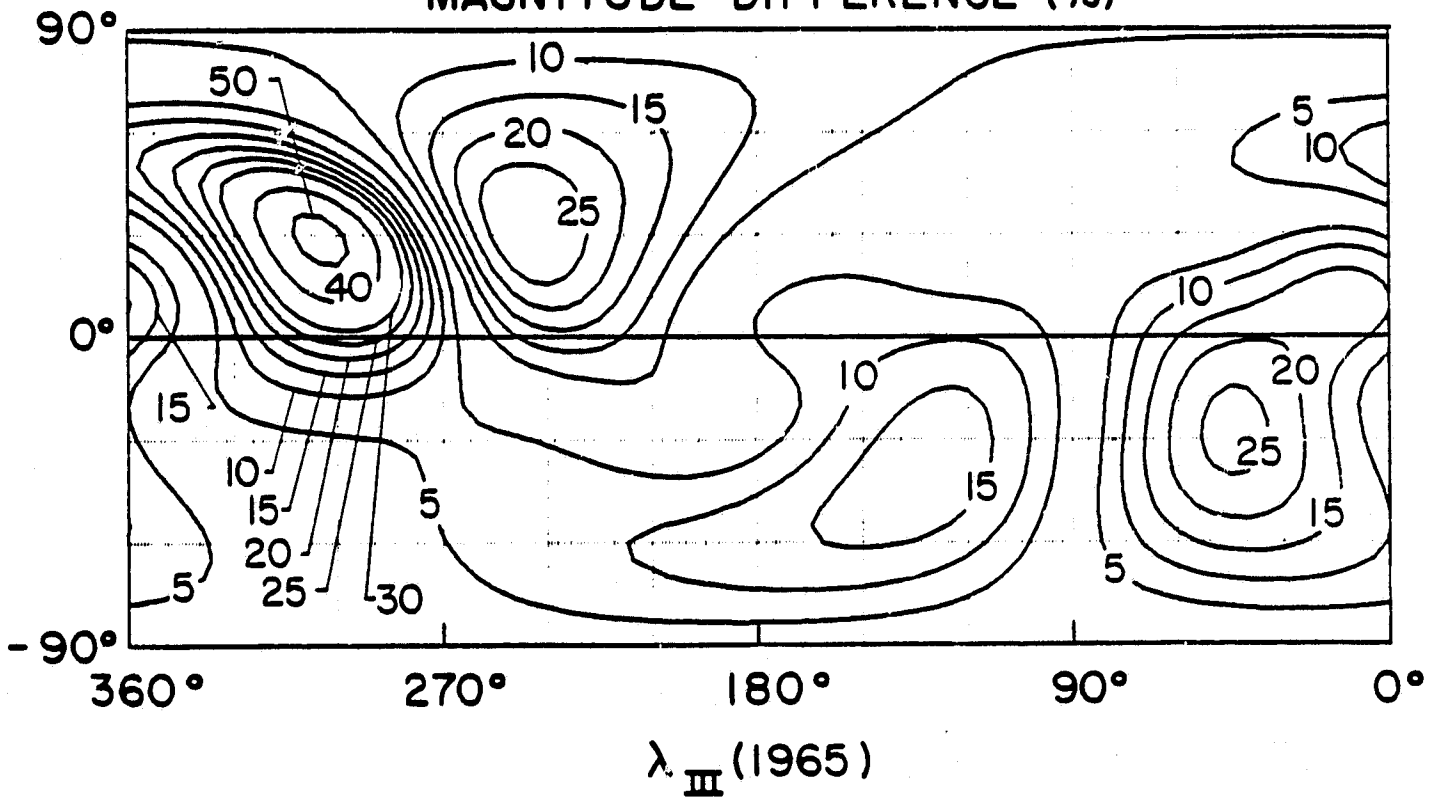## MODEL DIFFERENCES JPL 15 EVS, SHA 23

ANGLE DIFFERENCE (DEG.)

MAGNITUDE DIFFERENCE (%)

λ_{III} (1965)

1. Report No. TM 82146	2. Government Accession No.	3. Recipient's Catalog No.
4. Title and Subtitle Magnetic Field of Jupiter: A Generalized Inverse Approach		5. Report Date June 1981
		6. Performing Organization Code 695
7. Author(s) J. E. P. Connerney		8. Performing Organization Report No.
9. Performing Organization Name and Address Goddard Space Flight Center Greenbelt, Maryland 20771		10. Work Unit No.
		11. Contract or Grant No.
		13. Type of Report and Period Covered Technical Memorandum
12. Sponsoring Agency Name and Address		
		14. Sponsoring Agency Code

15. Supplementary Notes

16. Abstract

The estimation of planetary magnetic fields from observations of the magnetic field gathered along a spacecraft flyby trajectory is examined with the aid of generalized inverse techniques, with application to the internal magnetic field of Jupiter. Model non-uniqueness resulting from the limited spatial extent of the observations and noise on the data is explored and quantitative estimates of the model parameter resolution are found. The presence of a substantial magnetic field of external origin due to the currents flowing in the Jovian magnetodisc is found to be an important source of error in estimates of the internal Jovian field, and new models explicitly incorporating these currents are proposed. New internal field models are derived using the vector helium magnetometer observations and the high field fluxgate observations of Pioneer 11, and knowledge of the external current system gained from the Pioneer 10 and Voyager 1 and 2 encounter.

17. Key Words (Selected by Author(s)) Jupiter, generalized inverse, magnetic field, Pioneer 11, Voyager 1 and 2	18. Distribution Statement

19. Security Classif. (of this report) U	20. Security Classif. (of this page) U	21. No. of Pages 51	22. Price*